

Article

Design and Characterization of Biomimetic Hybrid Construct Based on Hyaluronic Acid and Alginate Bioink for Regeneration of Articular Cartilage

Cristina Galocha-León ^{1,†} , Cristina Antich ^{2,3,4,5,6,†}, Beatriz Clares-Naveros ^{1,3} , Ana Voltes-Martínez ^{2,3,4,5,6}, Juan Antonio Marchal ^{2,3,4,5,6,*} and Patricia Gálvez-Martín ^{7,*} 

- ¹ Department of Pharmacy and Pharmaceutical Technology, Faculty of Pharmacy, University of Granada, E-18071 Granada, Spain; galochacristina@gmail.com (C.G.-L.); beatrizclares@ugr.es (B.C.-N.)
 - ² Biopathology and Regenerative Medicine Institute (IBIMER), Centre for Biomedical Research, University of Granada, E-18100 Granada, Spain; cantich@go.ugr.es (C.A.); ana.voltes@gmail.com (A.V.-M.)
 - ³ Instituto de Investigación Biosanitaria ibs.GRANADA, University Hospital of Granada, University of Granada, E-18100 Granada, Spain
 - ⁴ Department of Human Anatomy and Embryology, Faculty of Medicine, University of Granada, E-18012 Granada, Spain
 - ⁵ Excellence Research Unit “Modeling Nature” (MNat), University of Granada, E-18071 Granada, Spain
 - ⁶ BioFab i3D—Biofabrication and 3D (Bio) Printing Laboratory, University of Granada, E-18100 Granada, Spain
 - ⁷ R&D Human and Animal Health, Bioibérica S.A.U., E-08029 Barcelona, Spain
- * Correspondence: jmarchal@ugr.es (J.A.M.); pgalvez@bioiberica.com (P.G.-M.)
† These authors contributed equally to this work.

Abstract: Background/Objectives: Three-dimensional bioprinting technology has enabled great advances in the treatment of articular cartilage (AC) defects by the biofabrication of biomimetic constructs that restore and/or regenerate damaged tissue. In this sense, the selection of suitable cells and biomaterials to bioprint constructs that mimic the architecture, composition, and functionality of the natural extracellular matrix (ECM) of the native tissue is crucial. In the present study, a novel cartilage-like biomimetic hybrid construct (CBC) was developed by 3D bioprinting to facilitate and promote AC regeneration. **Methods:** The CBC was biofabricated by the co-bioprinting of a bioink based on hyaluronic acid (HA) and alginate (AL) loaded with human mesenchymal stromal cells (hMSCs), with polylactic acid supporting the biomaterial, in order to mimic the microenvironment and structural properties of native AC, respectively. The CBC was biologically in vitro characterized. In addition, its physicochemical characteristics were evaluated in order to determine if the presence of hMSCs modified its properties. **Results:** Results from biological analysis demonstrated that CBC supported the high viability and proliferation of hMSCs, facilitating chondrogenesis after 5 weeks in vitro. The evaluation of physicochemical properties in the CBCs confirmed that the CBC developed could be suitable for use in cartilage tissue engineering. **Conclusions:** The results demonstrated that the use of bioprinted CBCs based on hMSC-AL/HA-bioink for AC repair could enhance the regeneration and/or formation of hyaline cartilaginous tissue.

Keywords: hyaluronic acid; mesenchymal stromal cell; bioprinting; construct; cartilage tissue engineering



Citation: Galocha-León, C.; Antich, C.; Clares-Naveros, B.; Voltes-Martínez, A.; Marchal, J.A.; Gálvez-Martín, P. Design and Characterization of Biomimetic Hybrid Construct Based on Hyaluronic Acid and Alginate Bioink for Regeneration of Articular Cartilage. *Pharmaceutics* **2024**, *16*, 1422. <https://doi.org/10.3390/pharmaceutics16111422>

Academic Editors: Donato Cosco and Sandra Sánchez-Salcedo

Received: 2 September 2024

Revised: 1 November 2024

Accepted: 4 November 2024

Published: 7 November 2024



Copyright: © 2024 by the authors. Licensee MDPI, Basel, Switzerland. This article is an open access article distributed under the terms and conditions of the Creative Commons Attribution (CC BY) license (<https://creativecommons.org/licenses/by/4.0/>).

1. Introduction

Articular cartilage (AC) tissue injuries remain a major challenge in orthopedic surgery since its regenerative capacity is limited, given its poor cellularity and avascular nature [1,2]. A range of options such as medication, rest, physiotherapy, and surgery are currently used to treat cartilage damage and repair [3]. Focal lesions of AC are surgically treated using techniques such as the microfracture, the abrasion arthroplasty, the debridement, the implantation of allografts, autologous chondrocytes (ACIs), matrix-induced chondrocyte

transplantation (MACI), or autologous matrix-induced chondrogenesis (AMIC) [4–8]. Each of these methods has specific strengths and limitations [3,9,10]. Although the current clinical approaches have achieved limited success, these treatments often involve a limited recovery of joint function associated with the formation of inadequate tissue. Repair procedures after cartilage injury can lead to the excessive secretion and deposition of natural extracellular matrix (ECM) proteins that can result in fibrocartilage formation with lower mechanical strength than native hyaline cartilage [4,5,7,11–13]. Therefore, the regeneration of hyaline cartilage remains the fundamental goal in the treatment of cartilage injuries. Recently, tissue engineering has emerged as an interdisciplinary field focused on developing new therapeutic approaches for cartilage regeneration. This involves creating biological substitutes that can restore, maintain, or enhance the function of damaged tissue. Generally, this is performed by culturing the cells in a three-dimensional (3D) structure, which mimics the composition and architecture of the ECM of the native AC being developed in order to be locally implanted in the injured AC, triggering and supporting the regeneration process [14,15]. Three-dimensional bioprinting enables the manufacture of individualized scaffolds with controllable micro-structures that provide cells a suitable microenvironment, biochemical stimulus, and mechanical support, which would eventually facilitate cell behavior including growth, proliferation, and differentiation [16,17].

Bioinks, bioprintable materials used in 3D bioprinting processes, can be divided into two categories: scaffold-based bioinks and scaffold-free bioinks. In the scaffold-based bioink, cells are loaded into hydrogels or similar exogenous materials, which are then bioprinted to create 3D structures [18,19]. In contrast, scaffold-free bioinks are composed of aggregates such as tissue spheroids [20–22], cell pellet [23], and tissue strands [24], where cells are bioprinted without the necessity of an external biomaterial [18,19]. Numerous researchers have reported the manufacturing of biomimetic constructs from hydrogels loaded with living cells [25–34]. The hydrogels provide an appropriate biomimetic microenvironment for cell proliferation, migration, differentiation, and adhesion [35]. In addition, hydrogels are biocompatible and biodegradable and have rich water content, which supply a matrix that can resemble natural components of the native ECM of AC [26,27,36–42]. However, despite these advances, the use of hydrogels has limitations such as their variability to obtain adequate mechanical properties. For this reason, the bioprinting of biomimetic hybrid constructs by the simultaneous deposition of hydrogels loaded with living cells and supporting biomaterials may offer a novel and more suitable strategy generating 3D structures that mimic the structural and compositional heterogeneity of native AC [43,44].

The bioprinting of cartilage constructs is generally extrusion based, which is the most common and affordable bioprinting method [17,45,46]. Alternatively, inkjet [47,48], laser-induced forward transfer (LIFT) [49], and 3D bioprinting provide a higher resolution, though they come at a considerably higher cost [50]. Each of these methods has specific strengths, weaknesses, and limitations [51].

Among biomaterials used as cell carriers, hyaluronic acid (HA) is one of the most promising natural polymers for cartilage tissue engineering (CTE). In osteoarthritic chondrocytes, HA enhances cellular metabolic activity, thereby promoting biosynthesis at the cellular level [52–54], playing a critical role during chondrogenesis and maintaining cartilage homeostasis [55,56]. In addition, it has been demonstrated that HA plays a role in the migration and proliferation of chondrocytes through its interaction with specific cell surface receptors such as CD44 [57,58]. Several studies have demonstrated that HA improves cell functionality in both chondrocytes and mesenchymal stromal cells (MSCs), promoting the chondrogenic phenotype and hyaline-specific matrix deposition [32,59–64], as well as suppressing genes associated with cartilage inflammation [65]. Moreover, HA is one of the main glycosaminoglycan (GAGs) present in the cartilage ECM and exhibits suitable properties such as biocompatibility, biodegradability, and non-toxicity [66–68]. Despite these advantages, HA presents a limited gelation capacity, which results in poor rheological properties for maintaining cell suspension [69,70]. In this context, HA has been mixed with other biomaterials, such as alginate (AL), to develop more viscous formulations

suitable for use as bioinks [71,72]. AL is considered a gold standard in CTE due to its easy handling, excellent rheological properties for bioprinting, fast gelation kinetics, and abilities to preserve the rounded cell shape that is essential for promoting the chondrogenic phenotype [73–76]. Thus, HA and AL can be combined because HA promotes cellular activity, while AL provides the appropriate rheological properties for the bioprintability of the bioink.

Regarding the supporting biomaterials, thermoplastic polymers such as polylactic acid (PLA) are some of the most promising biomaterials in CTE [77]. PLA provides excellent mechanical properties, thermoplastic processability, and biological properties, such as biocompatibility and biodegradability, which are all strongly influenced by its stereochemistry and molecular weight [77]. PLA also has excellent bioresorption capabilities, allowing the integration of the polymer with host cells and tissues [78]. Upon contact with biological media, PLA is degraded by simply hydrolyzing the ester bond into lactic acid, which is converted into pyruvate in the tricarboxylic acid cycle and excreted in the form of carbon dioxide and water. These degradation products are either metabolized intracellularly or excreted through urine and breath [79]. This process is primarily influenced by the characteristics of the polymer such as crystallinity, molecular weight, etc., and the conditions of hydrolysis, including pH and temperature [80]. Numerous studies have demonstrated that PLA, when used as a scaffold in tissue engineering, supports cell proliferation and growth [81–83]; also, its low price makes it an ideal choice for use in 3D bioprinting [84–86]. Its use in biomedical applications has been approved by the main health agencies such as the Federal Drug Administration (FDA, USA) and the European Medicine Agency (EMA, European Union) [87]. Moreover, PLA has been reported to be an effective scaffold agent alone or in combination with hydrogels [84,88].

Furthermore, for the bioprinting of biomimetic hybrid construct, the selection of a cell type to combine with the hydrogels is crucial to formulate suitable bioinks. hMSCs are regarded as an attractive cell type for cartilage regeneration because they are multipotent stem cells, with a high capacity to self-renew and differentiate into various cell types, including cartilaginous lineage [89–92]. hMSCs have been used as therapeutic agents not only for their healing capacities performed through engraftment and differentiation but also through paracrine signaling. These cells are capable of secreting soluble factors, which are indispensable for the viability, proliferation, and differentiation of cells surrounding a defect, for hyaline cartilaginous ECM stimulation, and for modulating the immune response [93,94]. Moreover, hMSCs overcome the limitations of chondrocytes, which are the only highly specialized cells found in mature AC [95]. The main limitation of *in vitro* chondrocytes culture is the dedifferentiation that occurs during expansion in monolayer culture. Chondrocytes do not maintain their characteristic phenotype, and, as a result, their capacity to regenerate damaged cartilage is compromised [96]. Additionally, the scarcity of donor tissue presents another challenge to the use of autologous chondrocytes [12]. Among the sources of hMSCs, adipose tissue presents several advantages in comparison to other tissues (i.e., bone marrow), including easier access, less invasiveness [97], and a greater cell yield per unit of tissue as well [98]. Specifically, Hoffa's fat pad tissue has been demonstrated to contain multipotent and highly clonogenic adipose-derived stem cells [99,100].

To date, although much advancement in CTE strategies using 3D bioprinting systems have been reported, the bioprinting of a construct composed of a component of AC ECM, such as HA [101–104], with appropriate cell and structural properties that lead to hyaline cartilage tissue generation is still a challenge. Accordingly, in this study, we successfully developed a cartilage-like biomimetic hybrid construct (CBC) by 3D bioprinting as an effective approach to treat and support the regeneration of AC defects and to be applied affordably in the clinical area. The bioprinting of CBCs was performed using bioink, formulated with HA and AL and loaded with hMSCs, which were simultaneously bioprinted with PLA. Then, the CBC was crosslinked post-bioprinting with calcium chloride, obtaining a novel tissue-engineered product, which mimicked the environment and structural properties of

native AC. The functionality of the CBCs was evaluated by testing their cell viability, proliferation, and chondrocyte differentiation by protein and gene expression assays, comparing them with a control CBC based on hMSC-AL-bioink (a construct without HA). Moreover, the physicochemical properties of the designed CBCs such as their porosity, degradation, swelling, surface electrical properties, conductivity, and environmental scanning electron microscopy were assessed compared to cell-free CBCs.

2. Materials and Methods

2.1. Isolation and Culture of hMSCs

hMSCs were isolated from infrapatellar fat pad (IFP) of patients with osteoarthritis during joint replacement surgery. Ethical approval for the study was obtained from the Ethics Committee (number: 02/022010) of the Clinical University Hospital of Málaga, Spain. Informed patient consent was obtained for all samples used in this study. The fat tissue was minced and digested using an enzymatic solution of 1 mg/mL collagenase type IA (Sigma-Aldrich, St. Louis, MO, USA) and incubated on a shaker at 37 °C for 1 h. After digestion, collagenase was removed by a single wash in sterile phosphate-buffered saline (PBS; Sigma-Aldrich, St. Louis, MO, USA), followed by two additional washes in Dulbecco's Modified Eagle Medium (DMEM; Sigma-Aldrich, St. Louis, MO, USA) supplemented with 10% fetal bovine serum (FBS; Invitrogen, Waltham, MA, USA). The cell pellet was resuspended in DMEM (Sigma-Aldrich, St. Louis, MO, USA) containing 10% FBS and 1% penicillin/streptomycin (Sigma-Aldrich, St. Louis, MO, USA), added to tissue culture flasks, and cultured at 37 °C in 5% CO₂. At 80% of confluency, the cells were released with TriPLE (Invitrogen, Waltham, MA, USA) and subcultured. The medium was changed regularly every 3 days, and cells were used at passage 4 for all the experiments.

2.2. Preparation of hMSC-Loaded Bioinks

The hMSC-loaded AL/HA-bioink (hMSC-AL/HA-bioink) was developed by preparing a solution of AL (2% *w/v*; molecular weight of AL: 216.12 g/mol; Sigma) and HA (1% *w/v*; molecular weight: 1000 kDa; Bioiberica S.A.U., Barcelona, Spain). Both materials were sterilized by short cycle autoclaving prior to preparation. This technique has been previously shown to be effective in the sterilization of materials such as HA against some types of bacteria without affecting rheology, physicochemical properties, and printability [105], and it has also been used for the sterilization of the AL in other previous works [40,76,106]. hMSCs were then suspended in 1 mL of AL/HA-bioink at the concentration of 1×10^6 cells/mL, resulting in the hMSC-AL/HA-bioink, which was packed into syringes (3 cc). Additionally, two other bioinks were also formulated as controls: (i) an hMSC-AL-bioink without HA and (ii) an AL/HA-bioink without cells.

2.3. Biofabrication of Cartilage-like Biomimetic Hybrid Construct by 3D Bioprinting

The CBCs were bioprinted using REGEMAT V2 bioprinter (REG4Life, REGEMAT 3D, Granada, Spain) under aseptic conditions, as previously described [70] (Figure 1A). Briefly, PLA (Smart Materials 3D; tensile strength: 55.5 Mpa, specific gravity: 1.24 g/cm³, glass transition temperature: 60 °C, hardness: 85 shore D, diameter: 1.75 mm) was first deposited by head (at 200 °C) in a layer-by-layer manner to generate the framework, which was previously designed using software REGEMAT 3D designer v1.4.4 (porous cylinder-type structure, 5 mm high \times 10 mm wide structure; 375 μ m pore size) (Figure 1B,C). The selected pore size was based on previous studies of CTE (120–870 μ m) [107]. After depositing 4 layers of PLA, the hMSC-AL/HA-bioink was injected between PLA strands obtaining the constructs, which were then physically crosslinked using a bath of 100 mM calcium chloride (CaCl₂; Panreac, Barcelona, Spain), loaded into another syringe, for 30 min [108] (Figure 1C,D). In addition, two types of control constructs were bioprinted from hMSC-AL-bioink and AL/HA-bioink. It was biofabricated for as many constructs as needed for the following analytical studies.

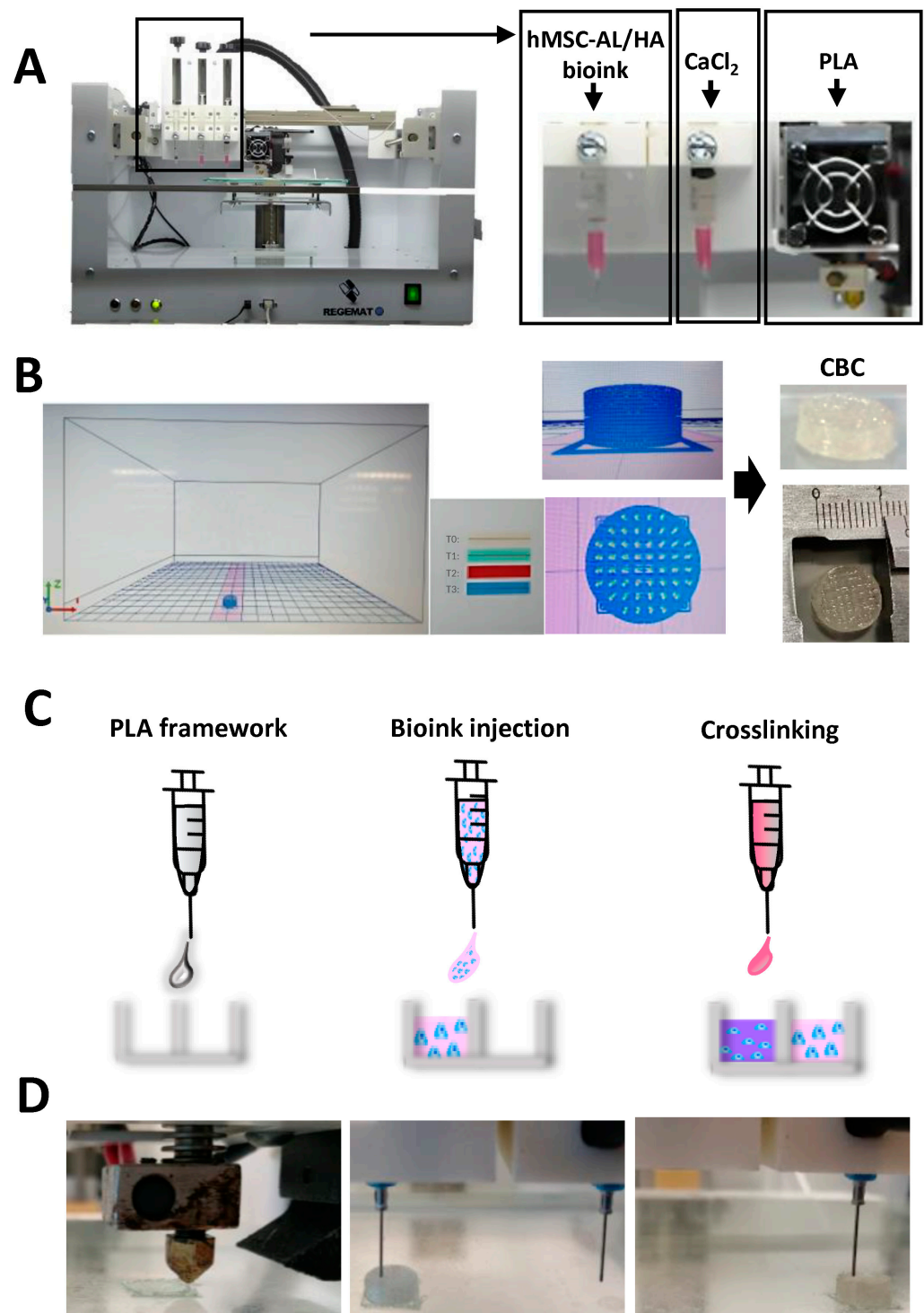


Figure 1. Three-dimensional bioprinting of CBCs based on hMSC-AL/HA-bioink. (A) REGEMAT Bioprinter system and bioinks. (B) Design of CBCs using REGEMAT software designer. (C) Scheme of dispensing and crosslinking of bioink in the PLA framework: hMSC-AL/HA-bioink (pink), calcium solution (blue), and crosslinked hMSC-AL/HA-bioink (purple). (D) Steps of biofabrication procedure of CBCs based on hMSC-AL/HA-bioink by 3D bioprinting.

2.4. CBC Maturation in Cell Culture

CBCs based on hMSC-AL/HA-bioink and control constructs based on hMSC-AL-bioink were cultured at 37 °C and 5% CO₂ atmosphere with high-glucose DMEM (Sigma) supple-

mented with 10% FBS (Lonza, Norwest, NSW, Australia) and 1% penicillin/streptomycin (Sigma) for a maximum of 5 weeks.

2.5. Flow Cytometry Analysis

The immunophenotype of hMSCs was analyzed by flow cytometry using fluorescence-activated cell sorter (FACS). Cells were washed and resuspended in PBS (Sigma) with 2% bovine serum albumin (BSA, Sigma) and 2 mM ethylenediaminetetraacetic acid (EDTA; Sigma). Cells were incubated in the dark for 30 min at 4 °C with the appropriate fluorochrome-conjugated monoclonal antibodies. The markers used were CD73-APC, CD90-FITC, CD105-PE, CD45-PerCP, CD19-APC, and HLA-DR-FITC (Miltenyi Biotec, Macquarie Park, NSW, Australia). After incubation, cells were washed in PBS and analyzed in a FACS Canto II cytometer (BD Biosciences, Franklin Lakes, NJ, USA).

2.6. Cell Differentiation STAINING Assay

For adipogenic, osteogenic, and chondrogenic differentiation, hMSCs were cultured for two weeks in Adipogenic MSC Differentiation Bullet kit, Osteogenic MSC Differentiation Bullet kit (Lonza), and NH ChondroDiff Medium (Miltenyi), respectively. Differentiated cell cultures were stained with Oil Red O (Amresco, Solon, OH, USA) for adipogenic differentiation, Alizarin Red (Lonza) for osteogenic differentiation, or Toluidine Blue (Sigma) for chondrogenic differentiation and imaged using an optical microscope (Leica DM 5500B; Leica Microsystems, L'Hospitalet de Llobregat, Spain).

2.7. Cell Viability Assay

The live/dead kit assay (Thermo Fisher Scientific, Waltham, MA, USA) was used to evaluate cell viability of cells embedded in CBCs and control constructs based on hMSC-AL-bioink, following manufacturer's instructions. Stained constructs from day 1, 3, 5, 7, 14, and 21 days in culture were observed using a confocal microscope (Nikon Eclipse Ti-E; Nikon Instruments Europe B.V., Amsterdam, The Netherlands) by two different filters. Green fluorescence was visualized in live cells and red fluorescence in dead cells. Confocal images were analyzed with Image J software (v. 1.52i, National Institutes of Health, Bethesda, MD, USA). The percentage of viable cells were obtained by counting six regions of each sample (n = 3).

2.8. Cell Proliferation

The proliferation rate of cells (n = 3) into CBCs and control constructs based on hMSC-AL-bioink were assessed by colorimetric Alamar Blue (aB) assay (Thermo Fisher Scientific) at initial and final culture time (day 0 and day 21, respectively), following manufacturer's instructions. Fluorescence intensity was measured with an excitation wave length of 530 nm and emission of 590 nm using a spectrophotometer (Synergy HT, BIOTEK, San Diego, CA, USA). The absorbance data were represented as fold increase to initial culture time.

2.9. Biochemical Assay

CBCs and control constructs based on hMSC-AL-bioink were digested in 1 mL of papain solution (125 mg/mL papain in 0.1 M sodium phosphate with 5 mM Na₂ EDTA and 5 mM cysteine HCl at pH 6.5) for 16 h at 60 °C, followed by centrifugation at 10,000 rpm for 5 min. The supernatant was used for chemical assay. The amount of GAGs was measured by the dimethylmethylene blue (DMMB) colorimetric assay. The supernatant was mixed with DMMB solution to bind GAGs. The GAG content was calculated based on a standard curve of chondroitin sulfate from shark cartilage (Sigma) at 530 nm using a microplate spectrophotometer and normalized with cell-free hybrid constructs. The DNA content was determined by a Hoechst assay and calculated using thymus DNA for a standard curve (Sigma). The supernatant was reacted with the Hoechst dye for 30 min in the dark. The intensity of fluorescence was screened with a 96-well plate reader (excitation at 360 nm and emission at 460 nm).

For type II collagen quantification, samples were digested by pepsin (1 mg/mL) in 0.5 N acetic acid for 48 h at 4 °C, followed by adding 1 mg/mL pancreatic elastase solution at 4 °C for 24 h. Finally, the samples were neutralized with 1 M Tris base. Insoluble material was removed by centrifugation at 10,000 rpm at room temperature for 5 min, and the supernatant was collected for assay. Quantitative analysis was performed using a commercially available type II collagen ELISA kit (Chondrex, Woodinville, WA, USA), according to manufacturer's instruction and measured on microplate spectrophotometer at 490 nm.

2.10. RT-PCR Analysis

Total messenger RNA (mRNA) of cells in CBCs and control constructs based on hMSC-AL-bioink (a construct without HA) was isolated using TriReagent (Sigma) and reverse transcribed into cDNA using the Reverse Transcription System kit (Promega, Madison, WI, USA). The quantitative real-time polymerase chain reaction (qRT-PCR) was conducted using a SYBR green master mix (Promega) according to the manufacturer's recommendations. Gene expression levels for aggrecan (*ACAN*), type II collagen (*COL2A1*), Sox transcription factor 9 (*SOX9*), type X collagen (*COL10A1*), and the RUNX2 gene (*RUNX2*) of the CBCs were normalized to the housekeeping gene glyceraldehyde 3-phosphate dehydrogenase (*GAPDH*) and showed a fold change relative to the value of the control constructs. The primer sequences are reported in a previous work [109]. All the samples were analyzed in triplicate for each gene.

2.11. Physicochemical Characterization

2.11.1. Porosity Analysis

The porosity of CBCs based on hMSC-AL/HA-bioink and cell-free CBCs based on AL/HA-bioink was determined by the solvent replacement method. Briefly, the dry samples were submerged in 20 mL absolute ethanol and then weighed after removing the excess of ethanol with tissue paper. The porosity of samples was obtained by the following equation [110,111]:

$$\text{Porosity} = \frac{W_2 - W_1}{\rho \times V} \times 100 \quad (1)$$

where W_2 is the weight of ethanol-absorbed samples, W_1 is the weight of dry samples, ρ is the ethanol density, and V is the volume of samples.

2.11.2. Swelling Test

The water uptake capacity of the CBCs based on hMSC-AL/HA-bioink and cell-free CBCs based on AL/HA-bioink was determined by swelling dried sample (with known weights) in 15 mL PBS (pH 7.4) at 37 °C. At predetermined intervals, samples were taken out, surface adsorbed water was removed by filter paper, and the wet weight was recorded. Each measure was carried out in triplicate. The swelling ratio was calculated as follows [112]:

$$\text{Swelling ratio (\%)} = \frac{W_s - W_d}{W_d} \times 100 \quad (2)$$

where W_s is the weight of the samples at the swelling state, and W_d is the initial mass of dried samples.

2.11.3. In Vitro Degradation Analysis

Before beginning in vitro degradation, CBCs based on hMSC-AL/HA-bioink and cell-free CBCs based on AL/HA-bioink were pre-wetted by immersion in PBS (pH = 7.4 ± 0.05) at 37 °C. Once equilibrium was reached, samples were weighed and recorded as W_0 . Samples were then incubated in 15 mL PBS at 37 °C. At specific time intervals, samples were removed and dried in a vacuum oven at 50 °C for 60 min, and their dry weight

was recorded. The samples were then returned to containers containing PBS [113]. The degradation (%) was calculated in triplicate according to the following equation [114]:

$$\text{Degradation ratio (\%)} = \frac{W_0 - W_t}{W_0} \times 100 \quad (3)$$

where W_0 is the initial mass of sample, and W_t is the mass of degraded sample measured at time t after drying at 50 °C in vacuum oven for 60 min.

2.11.4. Surface Electrical Properties

Sample preparation for zeta potential (ζ) and conductivity analysis of CBCs based on hMSC-AL/HA-bioink and cell-free CBCs based on AL/HA-bioink was performed as previously reported [43]. Briefly, samples were dried (10 mg dried mass) at 50 °C for 24 h. Then, they were suspended in double-distilled water and sonicated for 1 h at 50% frequency for further analysis. ζ was determined by electrophoresis measurements using a Zetasizer Nano ZS (Malvern Instruments Ltd., Malvern, UK). Furthermore, the surface electrical properties of samples as a function of pH variation (from 4 to 8, at constant 10^{-3} M KNO_3 concentration) and ionic strength (from 10^{-1} to 10^{-5} M KNO_3 , at pH = 6) were studied. Values are reported as the mean \pm SD ($n = 9$).

On the other hand, electrical conductivity of CBCs based on hMSC-AL/HA-bioink and cell-free CBCs based on AL/HA-bioink was measured with a conductometer Crison EC-Meter BASIC 30+ (Crison Instruments, Alella, Barcelona, Spain). An electrode was dipped into a glass vial of sample. Data were expressed as mean \pm SD ($n = 3$).

2.12. Scanning Electronic Microscopy (SEM)

To analyze internal microstructure of CBCs based on hMSC-AL/HA-bioink and cell-free CBCs based on AL/HA-bioink, the samples were fixed in cold 2.5% glutaraldehyde and rinsed in PBS, followed by a dehydration process through a graded series of ethanol (30–100%), and finally critically point-dried in an Emscope CPD 750 critical point dryer. Hybrid constructs were attached to aluminum SEM specimen mounting stubs (Electron Microscopy Sciences, Hatfield, PA, USA) and sputter-coated with a gold palladium alloy using a Sputter Coater 108 Auto. Finally, samples were examined using a scanning electron microscope eSEM (FEI Quanta 400, OR, USA) and a field emission scanning electron microscope JSM-7001F (JEOL Ltd., Tokyo, Japan). Images were taken at several magnifications.

2.13. Mechanical Testing of the Scaffolds

The compression modulus was measured using a universal testing machine (AGS-X Shimadzu, Kyoto, Japan) at a constant approaching speed from 0 to 0.1 mm. Measurements were conducted under controlled temperature and humidity conditions to minimize potential variations in material properties ($n = 5$).

2.14. Statistical Analysis

All data were represented as mean \pm SD. The two-tailed Student's t -test was used to determine differences between conditions. p -values < 0.01 (**) and < 0.05 (*) were considered statistically significant in all cases.

3. Results

3.1. CBC Biofabrication

The biofabrication of CBCs was based on a co-deposition of bioink formulated from HA and AL loaded with hMSCs mimicking the microenvironment and composition of the ECM of native AC with a PLA framework used as the mechanical support of the structure. CBCs based on hMSC-AL/HA-bioink, control constructs based on hMSC-AL-bioink, and cell-free CBCs based on AL/HA-bioink were successfully bioprinted by the combination of two procedures, Fused Deposition Model (FDM) and Injection Volume Filling (IVF), which are incorporated in the REGEMAT 3D V2 system. Each bioink was injected between PLA

frames in a layer-by-layer manner, resulting in a 5 mm high \times 10 mm wide structure. Then, constructs were immediately crosslinked with a calcium chloride bath (Figure 1C).

3.2. Flow Cytometry Analysis

Following the recommendation of the International Society for Cellular Therapy (ISCT), the hMSCs were characterized according to the minimal criteria for defining multipotent mesenchymal stromal cells. Flow cytometry analysis of the hMSCs revealed a high expression of CD90 (99.47%), CD73 (99.50%), and CD105 (99.89%) markers while showing a negative or low expression of CD45 (0.51%), CD19 (2.17%), and HLA (0.01%) markers (Figure 2).

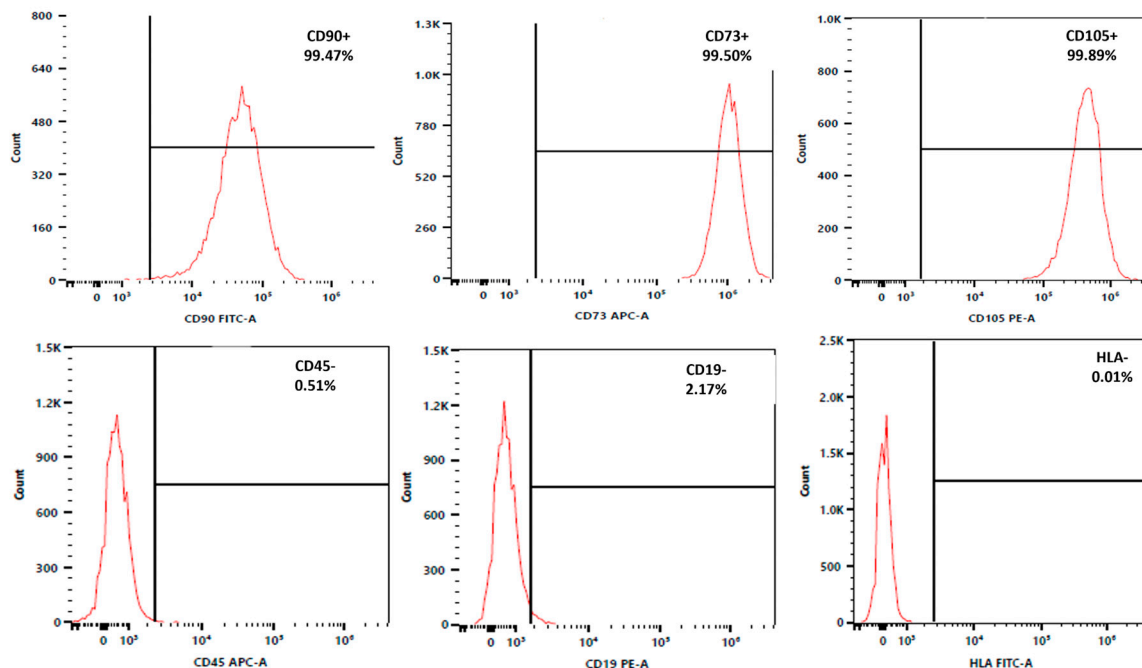


Figure 2. Phenotypic characterization of hMSCs. FACS characterization of hMSCs showed a positive expression of the surface markers CD90, CD73, and CD105 and negative or low expression of CD45, CD19, and HLA.

3.3. Cell Differentiation Staining Assay

The plasticity potential of the isolated cells was assessed to evaluate their ability to differentiate into chondrocytes, adipocytes, and osteoblasts. hMSCs were cultured under standard in vitro differentiating conditions for two weeks. Adipogenic differentiation was confirmed by the presence of lipid deposits stained with Oil Red. Osteogenic differentiation was determined by calcific deposition using Alizarin Red S staining. Chondrogenic differentiation was assessed by the presence of proteoglycans stained with Toluidine Blue. Thus, cells isolated from the IFP demonstrated the ability to differentiate into various mesenchymal tissue types, including adipocytes, chondrocytes, and osteoblasts (Figure 3).

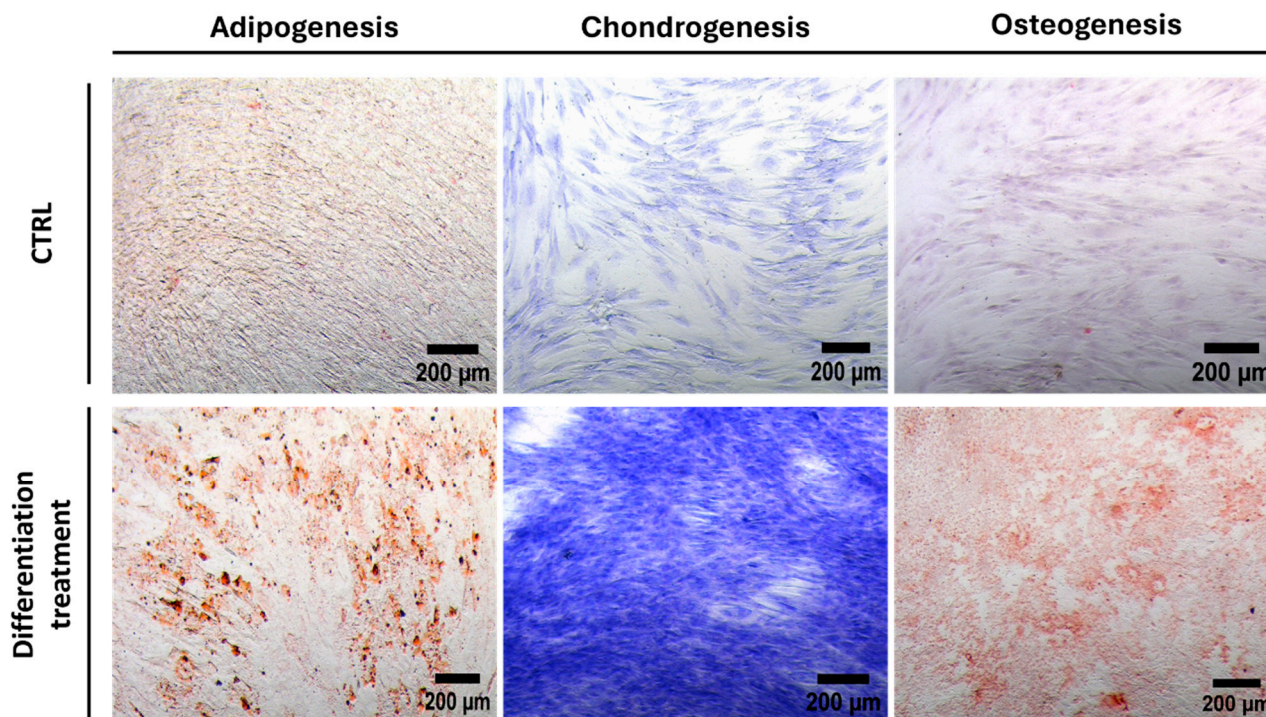


Figure 3. Cell differentiation staining assay. The differentiation potential of hMSCs obtained from IFP towards osteogenic, adipogenic, and chondrogenic lineage was confirmed by Alizarin red S, Oil Red O, and Toluidine Blue staining, respectively. Scale bar: 200 μm . Images were taken at 10 \times magnification.

3.4. Cell Viability

The viability of hMSCs in the CBC based on hMSC-AL/HA-bioink and in the control constructs based on hMSC-AL-bioink were analyzed at day 1, 3, 5, 7, 14, and 21 using life/dead staining assay. Confocal images showed a uniform distribution of cells within the CBC and in the control construct for the entire study period. hMSCs were embedded throughout the AL and AL/HA bioinks between the PLA strands (Figure 4A), being the majority viable cells (green-stained cells). After the bioprinting process (day 1), around 90% of living cells in the CBC and more than 80% of living cells in the control construct were observed. Long-term analysis also indicated that cell viability remained high (>85%) throughout the 14 days in the culture, slightly increasing from days 1 to 3 (Figure 4B). There is a significant difference in the control group between days 3, 7, and 21 compared to day 1. Additionally, significant differences were observed between the control construct group and the CBC groups, but only at day 21.

3.5. Cell Proliferation

Cell proliferation in CBCs based on hMSC-AL/HA-bioink and control constructs based on hMSC-AL-bioink was analyzed at initial and final time points of culture. Figure 4C shows that the proliferation rate of cells in CBCs is equal or comparable to the control constructs at both 0 and 21 days. After 21 days, cells exhibited an increase in growth in comparison to day 0. Although there were no significant differences between the control constructs and CBCs, significant differences were observed within each group over time, i.e., the metabolic activity of the cells increases over time for both conditions.

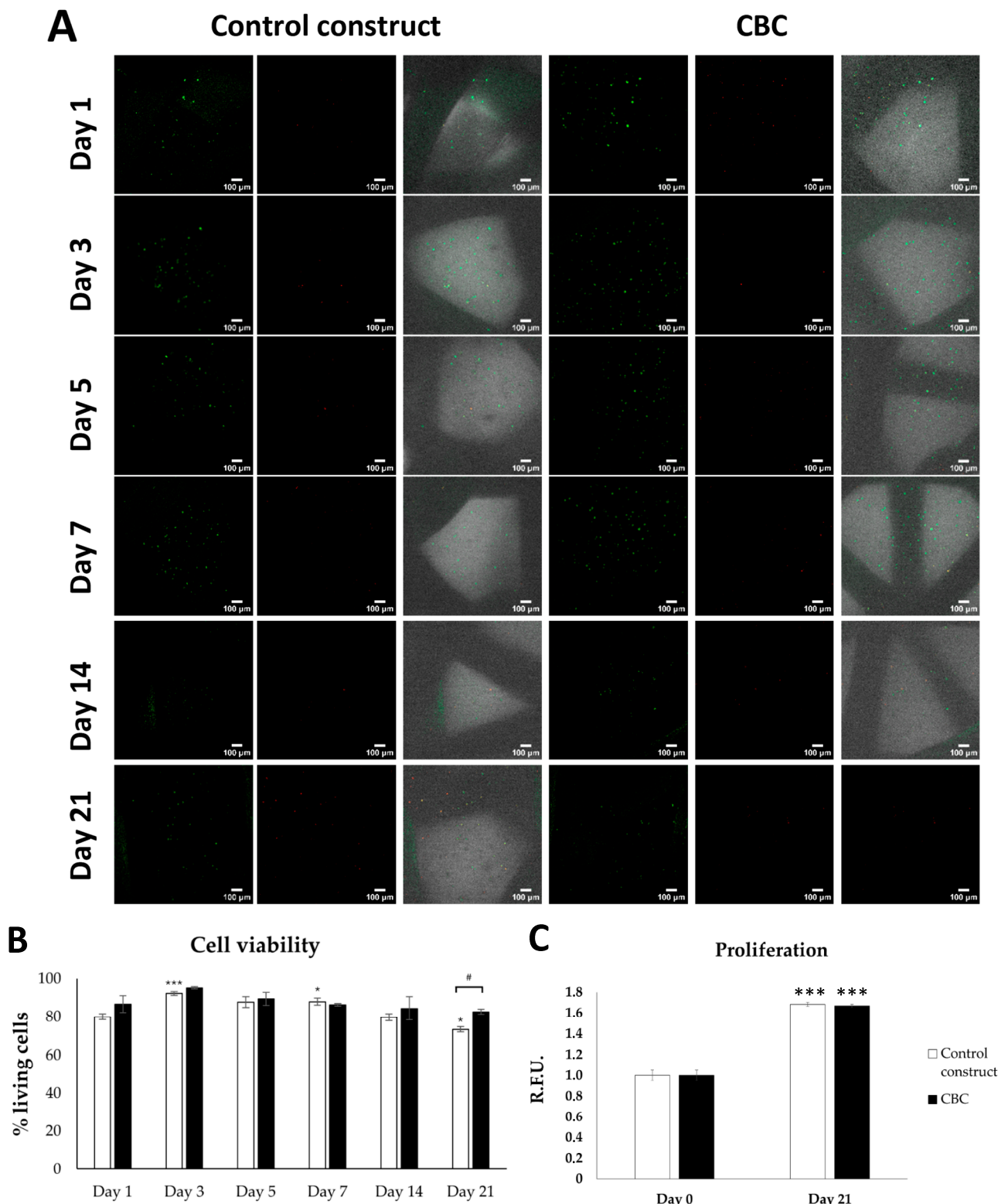


Figure 4. Cell viability and proliferation of hMSCs in control constructs based on hMSC-AL-bioink and CBCs based on hMSC-AL/HA-bioink. (A) Representative image of hMSCs in control constructs and CBCs after 1, 3, 5, 7, 14, and 21 days in culture, showing live (green) and dead (red) cells. (B) Percentage of hMSC viability in control constructs and CBCs with respect to time in culture. (C) Cell proliferation inside the CBCs based on hMSC-AL/HA-bioink (black) and control constructs based on hMSC-loaded AL-bioink (white). Error bars represent standard deviations ($n = 3$). (*) $p < 0.05$; (***) $p < 0.005$; (#) $p < 0.05$. Scale bar: 100 μm .

3.6. Chondrogenesis of hMSCs in CBCs

The capacity of hMSC-AL/AH-bioink to enhance chondrogenic differentiation and, therefore, cartilage formation in hybrid constructs was evaluated. Figure 5A shows the gene expression of hMSCs in CBC based on hMSC-AL/HA-bioink, after 5 weeks in culture, compared to hMSCs in control constructs based on hMSC-AL-bioink (without HA). For that, *COL2A1*, *ACAN*, *SOX9*, *COL10A1*, and *RUNX2* genes were analyzed. Results from qPCR analysis revealed an increase in mRNA levels of hyaline cartilage-specific genes such as *COL2A1*, *ACAN*, and *SOX9* from hMSCs bioprinted in CBCs based on hMSC-AL/HA-bioink in comparison to those bioprinted in the control group based on hMSC-AL-bioink, while the expression of the hypertrophic marker gene *COL10A1* was decreased in CBCs. The results for *RUNX2* expression (an essential transcription factor for osteoblast differentiation) showed a slight decrease in CBCs. No significant differences were observed in the expression of any of the genes ($p > 0.05$).

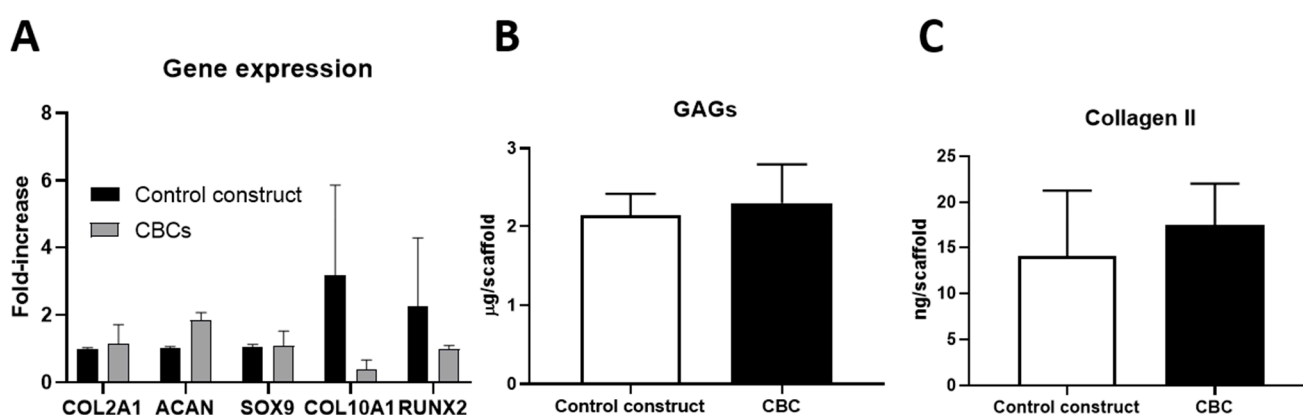


Figure 5. Chondrogenesis of hMSCs in CBCs based on hMSC-AL/HA-bioink and in control constructs based on hMSC-AL-bioink after 5 weeks in culture. (A) Gene expression levels of hyaline-specific chondrogenic marker genes (*COL2A1*, *ACAN*, and *SOX9*) and other genes such as *COL10A1* and *RUNX2* from cells in CBCs based on hMSC-AL/HA-bioink compared to cells of control constructs. (B) Quantitative analysis of GAGs. (C) Quantitative analysis type II collagen in the total extract per construct. Values represent mean \pm SD ($n = 3$).

hMSC chondrogenic differentiation was also analyzed at the protein level by measuring the production of the main components of chondrogenic matrix (GAGs and collagen II) after 5 weeks in culture. Results from biochemical assays indicated that GAG content in CBC based on hMSC-AL/HA-bioink (2.31 $\mu\text{g}/\text{construct}$) was slightly higher than those in the control construct based on hMSC-AL-bioink (2.15 $\mu\text{g}/\text{construct}$). Similarly, the amount of type II collagen was also higher in CBC based on hMSC-AL/HA-bioink (17.4 $\text{ng}/\text{construct}$) compared to the control construct (14.0 $\text{ng}/\text{construct}$), but, in both cases, such difference was not significant ($p > 0.05$) (Figure 5B,C).

3.7. Physicochemical Characterization of CBCs

The physicochemical characterizations of CBCs based on hMSC-AL/HA-bioink and cell-free CBCs based on AL/HA-bioink were conducted to evaluate whether the addition of cells modified the characteristics of the CBCs.

3.7.1. Porosity

Porosity is an important characteristic of constructs for TE, as it influences degradation, swelling capacity, and mechanical properties. The porosity of CBCs based on hMSC-AL/HA-bioink was higher than cell-free CBCs based on AL/HA-bioink, measuring $18 \pm 2.4\%$ and $2 \pm 0.9\%$, respectively.

3.7.2. Swelling Test

The water absorption ability was evaluated by immersing the samples in PBS at 37 °C for 120 days. Figure 6 shows the swelling behavior of CBCs based on hMSC-AL/HA-bioink and cell-free CBCs based on AL/HA-bioink. Low rates of swelling in both CBCs based on hMSC-AL/HA-bioink and cell-free constructs can be seen. The maximum swelling rate of CBCs based on hMSC-AL/HA-bioink was reached after 3 h, with a swelling percentage of $3.0 \pm 0.4\%$, whereas the cell-free constructs reached their maximum swelling after 24 h, with a swelling percentage of $5.4 \pm 0.5\%$. Afterward, the samples started to lose weight, and their swelling ratio seemed to stabilize with time.

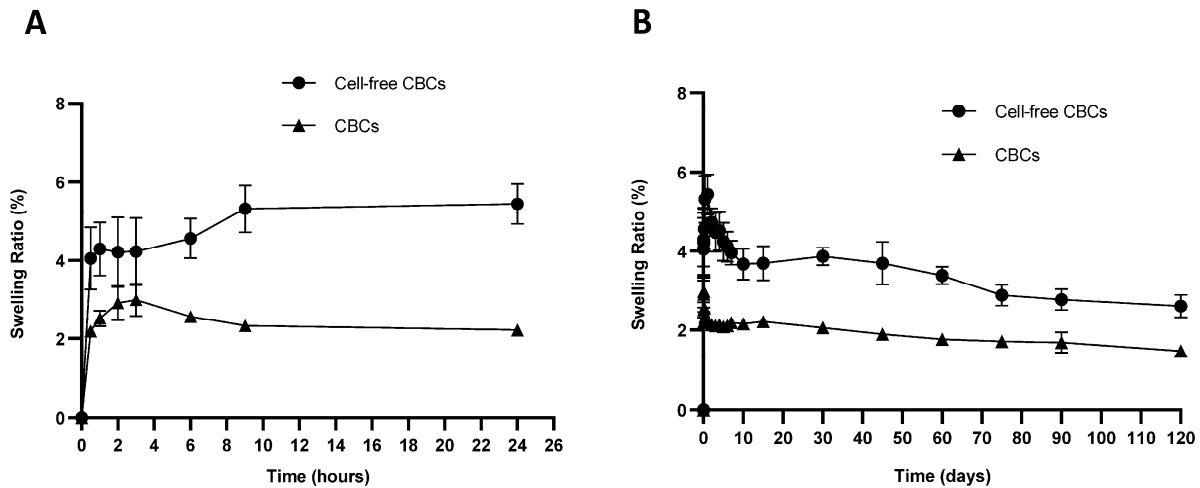


Figure 6. Swelling ratio of CBCs based on hMSC-AL/HA-bioink and cell-free CBCs based on AL/HA-bioink. (A) Swelling ratio at pH 7.4 and 37 °C after 24 h. (B) Swelling ratio at pH 7.4 and 37 °C after 120 days. Values represent mean \pm SD (n = 3).

3.7.3. In Vitro Degradation Analysis

The degradation of CBCs based on hMSC-AL/HA-bioink and cell-free CBCs based on AL/HA-bioink was expressed as the percentage of weight loss (Figure 7). This was evaluated by measuring the weight change of the samples after immersion in PBS at 37 °C for 120 days. The results indicate low percentages of degradation for both CBCs based on hMSC-AL/HA-bioink and cell-free CBCs based on AL/HA-bioink after 120 days of incubation. The degradation profile was higher for CBCs based on hMSC-AL/HA-bioink, with a weight loss of $8.8 \pm 0.6\%$, compared to $5.4 \pm 1.6\%$ for the cell-free CBCs.

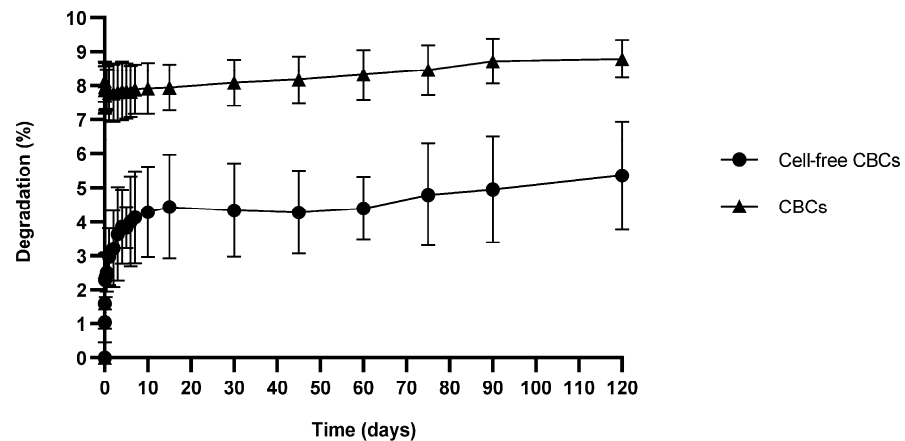


Figure 7. Degradation percentage of CBCs based on hMSC-AL/HA-bioink and cell-free CBCs based on AL/HA-bioink at pH 7.4 and 37 °C. Values represent mean \pm SD (n = 3).

3.7.4. Surface Electrical Properties and Conductivity Analysis

The electrophoretic characterization of CBCs based on hMSC-AL/HA-bioink and cell-free CBCs based on AL/HA-bioink is depicted in Figure 8. It can be observed a negative ζ ionic strength range both in CBCs based on hMSC-AL/HA-bioink and cell-free CBCs based on AL/HA-bioink (Figure 8A). The ζ showed a dependence on the ionic strength, with a slight decrease in negative ζ as KNO_3 concentration increased in both cases. Results of ζ ranged from -8.2 ± 1.4 mV to -25.1 ± 2.9 mV and -8.3 ± 0.8 mV to -26.4 ± 2.1 mV for CBCs based on hMSC-AL/HA-bioink and cell-free CBCs based on AL/HA-bioink, respectively. On the other hand, Figure 8B shows the ζ values at different pHs ranging from 4 to 8 in the presence of 10^{-3} M KNO_3 concentration at 25°C . A negative ζ was maintained across the pH range for both CBCs based on hMSC-AL/HA-bioink and cell-free CBCs based on AL/HA-bioink. The ζ (in an absolute value) followed an increase as pH increased from -11.2 ± 1.6 mV to -20.2 ± 1.5 mV for CBCs based on hMSC-AL/HA-bioink and from -9.1 ± 0.6 mV to -20.4 ± 1.4 mV for cell-free CBCs based on AL/HA-bioink.

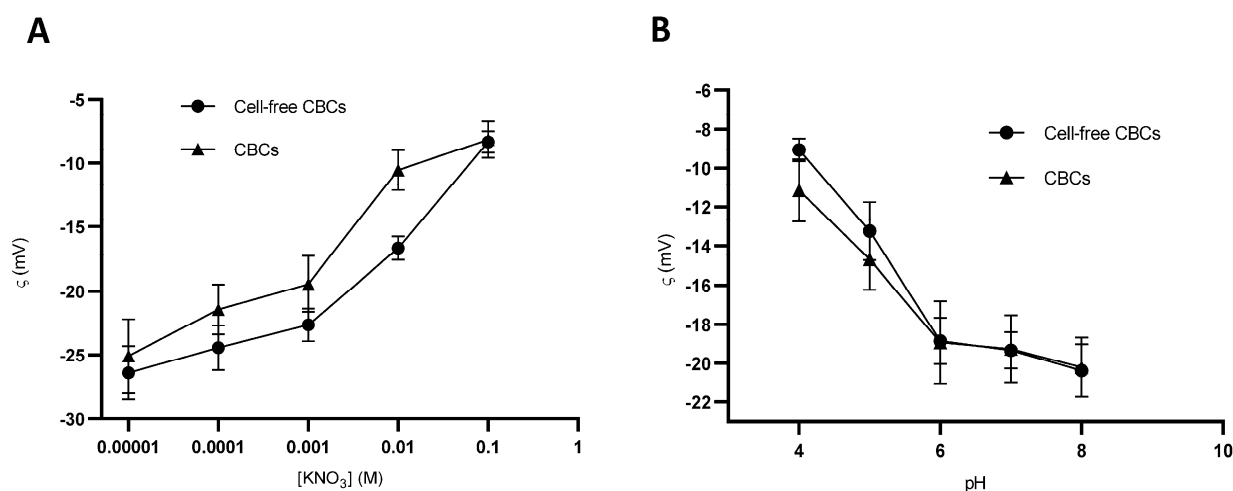


Figure 8. Zeta potential (ζ , mV) of CBCs based on hMSC-AL/HA-bioink and cell-free CBCs based on AL/HA-bioink. (A) ζ as a function of ionic strength at pH = 6 at 25°C . (B) ζ as a function of pH in the presence of 10^{-3} M KNO_3 concentration at 25°C . Values represent mean \pm SD ($n = 9$).

Finally, the conductivity values for CBCs based on hMSC-AL/HA-bioink and cell-free CBCs based on AL/HA-bioink were 160.0 ± 2.0 $\mu\text{S}/\text{cm}$ and 75.7 ± 5.0 $\mu\text{S}/\text{cm}$, respectively. These results indicated that the incorporation of hMSCs can greatly improve the conductivity of CBCs.

3.8. SEM Microscopy Analysis

The microstructure of CBCs based on hMSC-AL/HA-bioink and cell-free CBCs was analyzed by SEM. Images were taken on day 0, 7, and 21 with the optical microscope. Figure 9 shows the internal distribution of the main components in bioprinted constructs. SEM images of CBC based on hMSC-AL/HA-bioink revealed the presence of hMSCs, while no cells are visible in cell-free CBCs. The hydrogel within the constructs is clearly observable in the $150\times$ magnification images. Over time, the micrographs showed improved cell adhesion and cell growth in the constructs (Figure 9N,P,R).

3.9. Mechanical Test

The mechanical properties of scaffolds are crucial in the development of an effective artificial substitute. The ability of a construct to withstand deformation under an applied load is known as elastic or Young's modulus (E). The result obtained in this test shows that the CBCs have a Young's modulus of 4.069 ± 0.567 MPa. This result indicates that

the CBCs possess adequate stiffness to potentially function effectively as a scaffold in tissue-engineering applications.

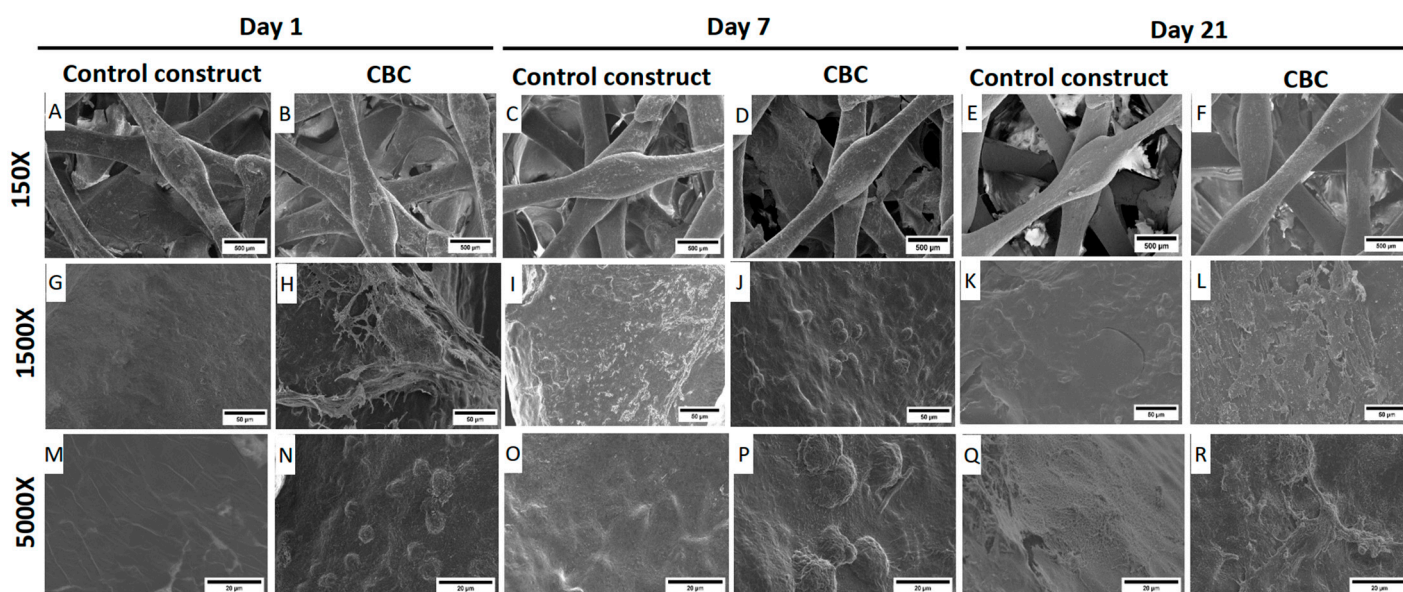


Figure 9. SEM microscopy analysis of hMSCs in constructs. (A,G,M) Cell-free CBCs based on AL/HA-bioink in cell culture conditions after 1 day. (B,H,N) CBCs based on hMSC-AL/HA-bioink in cell culture conditions after 1 day. (C,I,O) Cell-free CBCs based on AL/HA-bioink in cell culture conditions after 7 days. (D,J,P) CBCs based on hMSC-AL/HA-bioink in cell culture conditions after 7 days. (E,K,Q) Cell-free CBCs based on AL/HA-bioink in cell culture conditions after 21 days. (F,L,R) CBCs based on hMSC-AL/HA-bioink in cell culture conditions after 21 days. Images were taken at 150 \times (A–F; scale bar: 500 μ m), 1500 \times (G–L; scale bar: 50 μ m), and 5000 \times (M–R; scale bar: 20 μ m).

4. Discussion

Three-dimensional bioprinting technology offers a therapeutic alternative in the treatment of cartilage injuries [115]. The bioprinting of biomimetic hybrid constructs through the controlled and simultaneous deposition of hydrogels, as cell carriers, and thermoplastic polymers, as scaffolding biomaterials, has been demonstrated to be the most suitable strategy for cartilage regeneration. The selection of suitable biomaterials for bioprinting a construct is essential, especially for the formulation of cell-laden bioinks. Bioinks are mainly formulated from hydrogels, which not only must provide a good biomimetic environment for cells to grow and differentiate correctly but also must protect them from damaging conditions generated during the 3D bioprinting process, such as heat and shear stress [34,116,117], ensuring cell viability within the construct at the time of its implantation. Supportive biomaterials must also have good biodegradability and appropriate porosity to ensure cellular penetration and the adequate diffusion of nutrients to cells. In addition, a construct should provide mechanical properties consistent with the damage tissue to treat [118,119]. Tissue bioprinting presents several challenges for its translation into clinical practice, primarily in sourcing patient-derived cells to minimize immune rejection. This process involves complexities in cell collection and expansion and in ensuring adequate cell counts for successful bioprinting and tissue maturation. Additionally, ensuring compatibility for long-term storage and addressing sourcing and batch variability of bioinks are critical issues. Advancements in bioprinting techniques and the standardization of processes are essential for scalable production. Ethical, legal, and social considerations surrounding bioprinted tissues also need thorough deliberation [120,121].

In this study, a CBC was developed from hMSC-AL/HA-bioink. This bioink combined HA with AL, which is considered one of the most appropriate biomaterials for

bioprinting [31,122,123]. The formulation of the hMSC-AL/HA-bioink, composed of 1% HA and 2% AL, was selected based on our previous study in which it was demonstrated to better promote chondrogenic phenotype and hyaline-cartilage-specific matrix formation in comparison to other combinations [70].

For that, we successfully developed a novel CBC by 3D bioprinting to facilitate and promote cartilage regeneration. The CBCs were biofabricated by co-printing the hMSC-AL/HA-bioink with a supporting thermoplastic biomaterial, such as PLA, to mimic both the environment and mechanical properties of native AC. In our previous study, we demonstrated that the mixture of HA with AL has excellent biological and rheological properties to be used as cell-carrier biomaterial for CTE bioprinting, including a cartilage-like environment, printability, and gelling abilities [70]. In term of cells, hMSCs from adipose tissue represent an ideal cell source to treat cartilage defects, not only due to their potential to differentiate into cartilage lineage but also due to their easy accessibility and abundance in the body, overcoming the limitations associated with chondrocytes [124].

The ISCT proposed minimal criteria to define hMSCs. First, hMSCs must be plastic-adherent when maintained in standard culture conditions. Second, hMSC must express CD105, CD73, and CD90 and lack the expression of CD45, CD34, CD14, CD11b, CD79 α , or CD19 and HLA-DR surface molecules. Third, hMSCs must differentiate into osteoblasts, adipocytes, and chondroblasts in vitro [125,126]. The fluorescence-activated cell sorting analysis of hMSCs showed a positive expression of the surface markers CD90, CD73, and CD105 and a negative expression of CD45, CD19, and HLA-DR. We also tested the plasticity potential of the isolated cells by examining their ability to differentiate into chondrocytes, adipocytes, and osteoblasts using Alizarin Red S, Oil Red O, and Toluidine Blue staining. Cells isolated from the IFP of patients with osteoarthritis were able to differentiate into adipocytes, chondrocytes, and osteoblasts. These results confirmed the minimal phenotypic pattern for the identification of hMSC cells and the differentiation potential of hMSCs. Representative images for the live/dead assay of CBCs based on hMSC-AL/HA-bioink clearly indicated that cells were viable, emphasizing the potential of hMSC-loaded bioink as a cell encapsulating hydrogel for the biofabrication of cartilage constructs. In accordance with our previous work, this fact could be explained through the shear thinning behavior described previously, which reduces shear stress causative of cell disruption [70]. The results confirmed that hMSC-AL/HA-bioink offered a cell-friendly environment, maintaining a high percentage of viability in CBC based on hMSC-AL/HA-bioink over 21 days in culture, as has been well documented in many studies [127]. In addition to rheological properties of hMSC-loaded AL/HA-bioink, this high cell viability would be attributed in part to the microstructure of the bioprinted construct. By the analysis of cell proliferation, a significant increase in cell growth over this period (21 days) in CBC based on hMSC-AL/HA-bioink in comparison to control constructs based on hMSC-loaded AL-bioink was also evidenced. These results are in accordance with other studies that reported the beneficial effect of HA on cell proliferation [59,128,129]. In terms of functionality, it was observed that the environment provided by hMSC-loaded AL/AH-bioink in CBC is influenced by the commitment of hMSCs to undergo chondrogenesis. Previous studies have demonstrated that AL can induce chondrogenic differentiation and promote the retention of the spheroidal shape of cells, which is the differentiated phenotype of chondrocytes [76,90,130]. Meanwhile, HA has been shown to independently induce chondrogenesis on hMSCs [131] and to drive chondrocyte regeneration when it was used as injected scaffold [14,132,133]. In this study, the addition of HA to AL has demonstrated a positive effect, improving the ability of hMSCs to differentiate and produce the main components of chondrogenic ECM (GAGs and collagen II). The analysis of gene expression showed an increase in the expression of mature chondrocyte genes (*COL2A1*, *ACAN*, and *SOX9*) in the presence of HA. In accordance with our results, a stimulatory effect on the synthesis of collagen II and GAGs has been observed through various mechanisms. This effect is expected to result from cell receptor binding with HA (i.e., CD44, hyaluronan-mediated motility receptor). Chondrocytes and hMSCs have membrane receptors capable of

binding to HA and, thus, being influenced by its presence [56]. Moreover, there was a trend towards a reduction in hypertrophic marker (COL10A1) and osteogenic marker (RUNX2). Type X collagen is located in hypertrophic cartilage and the calcified zone of articular cartilage. Hypertrophic chondrocytes directly promote changes of their surrounding matrix, which increases mineralization and reduces the elastic properties of the cartilage [134]. The low expression of COL10A1 observed suggests that the hMSCs are not differentiating towards a hypertrophic chondrocyte lineage, thereby reducing the risk that the regenerated cartilage will progress towards an undesirable phenotype that could compromise tissue functionality. Additionally, RUNX2 is a transcription factor of osteoblast differentiation; it plays a determinant role in the early osteogenic differentiation and has become a marker of early osteogenic differentiation [135]. The low expression of RUNX2 suggests that the cells are not progressing toward osteoblastic differentiation.

The knowledge of CBCs based on hMSC-AL/HA-bioink in comparison with the cell-free CBCs based on AL/HA-bioink is essential to predict if the presence of living cells inside the constructs can modify or alter their physicochemical characteristics [136]. The porosity, pore size, and pore-to-pore interconnectivity can facilitate the cellular migration and infiltration as well as the right flow nutrients and oxygen within the construct and metabolic waste disposal, creating a favorable environment for tissue regeneration [137–140]. In fact, our results showed that the addition of hMSCs led to an increase in porosity value, probably due to the spatial incorporation of the cells within the CBCs. These data were verified in SEM images, which revealed that the CBC based on hMSC-AL/HA-bioink, as well as the PLA framework that it contains, had enough large interconnected pores to allow the diffusion of nutrients, oxygen, and metabolism products within the cartilage matrix, which is essential for cell living and their growth. The porosity values of the PLA framework are in the range of values reported in previous studies about 3D scaffolds for CTE [107]. The SEM images showed the internal distribution of the main components in the bioprinted constructs and revealed the presence of hMSCs in the CBCs based on hMSC-AL/HA-bioink. After 21 days, CBCs based on hMSC-AL/HA-bioink improved cell adhesion and cell growth.

The ability to absorb liquid, or swelling, is an important property of constructs, as it is associated with the flow nutrients and oxygen through the material structure [141–143]. The low swelling data obtained may be due to a characteristic of PLA, which is a relatively hydrophobic thermoplastic polyester [144]. Cheng et al. also reported a low swelling ratio of the PLA scaffolds [145]. Despite this, the low swelling data did not compromise the cellular viability and probably contributed to prolonging the degradation process. Our results are similar to those obtained by Correira et al. They prepared freeze-dried composite scaffolds of chitosan and HA and showed low swelling values throughout the entire experiment. In addition, they demonstrated that the ratio between chitosan and HA significantly affected the scaffolds' swelling properties. Despite these results, they suggested that the developed scaffolds could have potential use in the regeneration of cartilaginous lesions [141].

The degradation rate of a construct is a critical element for the repair process. The ideal construct should be biodegradable and allows for remodeling as the new cartilage forms, substituting the damaged cartilage. The construct should exhibit progressive degradation that coincides with ECM deposition and accumulation and align with the restoration of new tissue or function [138,141]. In our study, the degradation showed low rates in the developed CBCs. This slow degradation rate may be a consequence of the poor biodegradability of PLA, as demonstrated by Nazeer et al. and Cheng et al. in their research [145,146]. PLA degrades through the hydrolysis of backbone ester groups, which is enhanced by enzymes and depends on the ability of water to diffusion into the polymer [144,147]. During hydrolysis, PLA is broken down into water-soluble monomers and oligomers, which are eventually decomposed into water and carbon dioxide and removed. This process is mainly influenced by the characteristics of PLA (such as crystallinity, molecular weight, monomer concentration, conformation, and porosity [80,148]), as well as the hydrolysis environment,

including pH, temperature, and other factors. To accelerate the degradation of PLA, methods such as blending, compounding, copolymerization, and surface modification have been studied [80]. Apart from that, the degradation rate of AL-based biomaterials is also affected by the molecular weight of AL. Essentially, a higher molecular weight reduces the number of reactive sites accessible for hydrolytic degradation, leading to a slower degradation rate [149]. On the other hand, the presence of hMSCs rendered CBCs more susceptible to degradation, likely due to increased hydrolysis induced by acidic conditions as a result of the metabolic activity of cells, as well as to a higher porosity and better accessibility of cleavage sites [141,150]. It can be observed that the degradation is affected by porosity, showing a direct relation between the porosity of constructs and degradation percentage. It is widely known that the porosity of scaffolds could influence the degradation rate [151,152]. Zhang et al. demonstrated that increasing the porosity of scaffolds leads to their higher and faster development compared to less porous scaffolds [153]. The results obtained in our work are in accordance with other studies related to cartilage regeneration that reported a low percentage of degradation similar to our data (~between 1 and 7%). Correia et al. reported a slow degradation rate and confirmed that the degradation increased with higher HA concentration [141]. Thus, CBCs based on hMSC-AL/HA-bioink could be used for CTE because *in vivo* tissue regeneration is a slow process [143].

The electrical properties could help to understand the cellular processes that occur on the surface of the constructs. It has been reported that the ζ can affect both static cell behavior and dynamic cell behavior [151,154]. The negative ζ observed could be attributed to the dominance of hydroxyl and carboxyl groups on the surface of HA and AL [155,156], as well as the presence of terminal carboxylic groups on the surface of PLA [157]. The ζ values obtained for the developed CBCs are in agreement with previous studies, where values gradually decreased with increasing pH, ranging from -2 mV to -35 mV, and recorded -18 mV at pH 7.4 [158]. AC has an intracellular pH of around 7.15 and a slightly acidic extracellular medium, around 6.6 [159]. Under physiological conditions, a value of ζ around 20 is observed. These ζ values mimic the negative charges of the GAG chains on the ECM. Negative charges attract water molecules into the ECM. This fact leads to an increase in the tension of the collagen network and contributes to the tension that the tissue can resist. Further, it will be useful to interact with positively charged proteins [160,161]. Conductivity can influence cell growth and differentiation; therefore, the use of biocompatible conductive polymers could create a favorable culture environment to promote cellular activities [162]. The high values of conductivity obtained in the CBCs based on hMSC-AL/HA-bioink may contribute to induce the specific differentiation of hMSCs, as well as to enhance the cell-to-cell communication and cell adhesion [163].

The elastic modulus of a scaffold could be related to the optimization of the bioprinting process and the homogeneity of the material, as mentioned earlier by Martínez-Moreno et al. [164]. The result obtained from the mechanical test of CBCs shows a relevant Young's modulus value compared to other biomaterials used in CTE. For example, in the study conducted by Petitjean et al. on healthy and unstressed AC, the elastic modulus of the native tissue varied between 0.25 and 3 MPa [165]. Although CBCs have a slightly higher Young's modulus (4.069 ± 0.567 MPa), this value suggests that the constructs are suitable for load-bearing in complex clinical applications, offering structural stiffness, functionality, and scaffold integration comparable to that of native tissue.

In summary, results from biological analyses demonstrated the beneficial effect of HA, as CBCs based on hMSC-AL/HA-bioink supported high viability, stimulated cell proliferation, and facilitated the chondrogenesis of hMSCs better than the control construct bioprinted from hMSC-AL-bioink, which is considered as the gold standard bioink for CTE [166–168]. From a physicochemical point of view, our CBCs have microarchitecture (morphology and porosity) with sufficient space for cell proliferation and surface characteristics (ζ and conductivity) that are suitable for controlling cell-to-cell and cell-to-material interactions. On the other hand, our results indicate that the developed CBCs exhibit slow degradation, which can be attributed to PLA. This slow degradation is desirable in cartilage

tissue regeneration applications. However, modeling the degradation processes in vivo may be needed to understand how they affect tissue regeneration. Furthermore, the low swelling observed in this material during our assay may affect the exchange of nutrients and oxygen through the material structure. Although our results did not compromise cellular viability, the degradation rate and swelling ratio could be improved by modifying the structural conformation, molecular weight, orientation, and crystallinity of PLA [169]. The degradation rate could also be increased by decreasing the molecular weight of the AL. Finally, in the future, we expect to investigate cartilage regeneration in vivo using these hybrid constructs in animal models to evaluate their potential for clinical application.

5. Conclusions

In conclusion, our results demonstrated that the use of bioprinted CBCs based on hMSC-AL/HA-bioink and thermoplastic PLA for AC repair could enhance the regeneration and/or formation of hyaline cartilaginous tissue. This is because CBC based on hMSC-AL/HA-bioink has been shown to provide a suitable environment for cell growth, despite it exhibiting similar benefits in terms of functionality to the control construct based on hMSC-AL-bioink, whose chondro-inductive properties, independently of other stimulating factors, have been already evidenced. In addition, the physicochemical properties of the CBCs based on hMSC-AL/HA-bioink have only been slightly altered compared to cell-free CBCs based on AL/HA-bioink, confirming that the artificial cartilage developed in this work could be suitable for use in CTE. To verify these assumptions, future long-term studies in vitro and in vivo should be carried out.

Author Contributions: Conceptualization: B.C.-N., J.A.M. and P.G.-M.; investigation: C.G.-L., C.A. and A.V.-M.; methodology: C.G.-L., C.A., B.C.-N., A.V.-M., J.A.M. and P.G.-M.; data analysis: C.G.-L., C.A., B.C.-N., A.V.-M., J.A.M. and P.G.-M.; funding acquisition: J.A.M., B.C.-N. and P.G.-M.; writing—original draft: C.G.-L., C.A. and A.V.-M.; writing—review and editing: C.G.-L., C.A., B.C.-N., A.V.-M., J.A.M. and P.G.-M. All authors have read and agreed to the published version of the manuscript.

Funding: This work was partially supported by the Ministerio de Economía, Industria y Competitividad (FEDER funds, project RTC-2016-5451-1) (to B.C.-N., J.A.M., and P.G.-M.), by the Ministry of Economy and Competitiveness, Instituto de Salud Carlos III (FEDER funds, projects DTS19/00143 and DTS17/00087), by the Consejería de Economía, Conocimiento, Empresas y Universidad de la Junta de Andalucía (P18-FR-2470, PYC20 RE 015 UGR, A-CTS-180-UGR20 and B-CTS-230-UGR18) (to J.A.M.), and by the Fundación Mutua Madrileña (project FMM-AP17196-2019) (to C.A. and J.A.M.). Additionally, it has been developed in the context of AdvanceCat with the support of ACCIÓ (Catalonia Trade & Investment; Generalitat de Catalunya) under the Catalanian European Regional Development Fund operational program, 2014–2020 (to P.G.-M.).

Institutional Review Board Statement: Not applicable.

Informed Consent Statement: Not applicable.

Data Availability Statement: The original contributions presented in the study are included in the article, further inquiries can be directed to the corresponding authors.

Conflicts of Interest: Patricia Gálvez-Martín is an employee from Bioibérica S.A.U. The remaining authors declare that the research was conducted in the absence of any commercial or financial relationships that could be construed as a potential conflict of interest.

References

1. Burry, H.C. Adult Articular Cartilage. *Proc. R. Soc. Med.* **1974**, *67*, 691.
2. Bhosale, A.M.; Richardson, J.B. Articular Cartilage: Structure, Injuries and Review of Management. *Br. Med. Bull.* **2008**, *87*, 77–95. [[CrossRef](#)] [[PubMed](#)]
3. Solanki, K.; Shanmugasundaram, S.; Shetty, N.; Kim, S.J. Articular Cartilage Repair & Joint Preservation: A Review of the Current Status of Biological Approach. *J. Clin. Orthop. Trauma* **2021**, *22*, 101602. [[PubMed](#)]
4. Abdel-Sayed, P.; Pioletti, D.P. Strategies for Improving the Repair of Focal Cartilage Defects. *Nanomedicine* **2015**, *10*, 2893–2905. [[CrossRef](#)] [[PubMed](#)]

5. Zylińska, B.; Silmanowicz, P.; Sobczyńska-Rak, A.; Jarosz, Ł.; Szponder, T. Treatment of Articular Cartilage Defects: Focus on Tissue Engineering. *In Vivo* **2018**, *32*, 1289–1300. [[CrossRef](#)] [[PubMed](#)]
6. Tamaddon, M.; Wang, L.; Liu, Z.; Liu, C. Osteochondral Tissue Repair in Osteoarthritic Joints: Clinical Challenges and Opportunities in Tissue Engineering. *Bio-Des. Manuf.* **2018**, *1*, 101–114. [[CrossRef](#)]
7. Lyon, R.; Liu, X.C. Future Treatment Strategies for Cartilage Repair. *Clin. Sports Med.* **2014**, *33*, 335–352. [[CrossRef](#)]
8. Malahias, M.A.; Kostretzis, L.; Megaloikononimos, P.D.; Cantiller, E.B.; Chytas, D.; Thermann, H.; Becher, C. Autologous Matrix-Induced Chondrogenesis for the Treatment of Osteochondral Lesions of the Talus: A Systematic Review. *Orthop. Rev.* **2020**, *12*, 8872. [[CrossRef](#)]
9. Cong, B.; Sun, T.; Zhao, Y.; Chen, M. Current and Novel Therapeutics for Articular Cartilage Repair and Regeneration. *Ther. Clin. Risk Manag.* **2023**, *19*, 85–502. [[CrossRef](#)]
10. Johnson, L.L. Arthroscopic Abrasion Arthroplasty: A Review. *Clin. Orthop. Relat. Res.* **2001**, *391*, S306–S317. [[CrossRef](#)]
11. Armiento, A.R.; Stoddart, M.J.; Alini, M.; Eglin, D. Biomaterials for Articular Cartilage Tissue Engineering: Learning from Biology. *Acta Biomater.* **2018**, *65*, 1–20. [[CrossRef](#)] [[PubMed](#)]
12. Revell, C.M.; Athanasiou, K.A. Success Rates and Immunologic Responses of Autogenic, Allogenic, and Xenogenic Treatments to Repair Articular Cartilage Defects. *Tissue Eng. Part B Rev.* **2009**, *15*, 1–15. [[CrossRef](#)] [[PubMed](#)]
13. Knutsen, G.; Drogset, J.O.; Engebretsen, L.; Grøntvedt, T.; Isaksen, V.; Ludvigsen, T.C.; Roberts, S.; Solheim, E.; Strand, T.; Johansen, O. A Randomized Trial Comparing Autologous Chondrocyte Implantation with Microfracture: Findings at Five Years. *J. Bone Jt. Surg. Ser. A* **2007**, *89*, 105–2112.
14. Huh, S.W.; Shetty, A.A.; Ahmed, S.; Lee, D.H.; Kim, S.J. Autologous Bone-Marrow Mesenchymal Cell Induced Chondrogenesis (MCIC). *J. Clin. Orthop. Trauma* **2016**, *7*, 153–156. [[CrossRef](#)] [[PubMed](#)]
15. Bryant, S.J.; Davis-Arehart, K.A.; Luo, N.; Shoemaker, R.K.; Arthur, J.A.; Anseth, K.S. Synthesis and Characterization of Photopolymerized Multifunctional Hydrogels: Water-Soluble Poly(vinyl alcohol) and Chondroitin Sulfate Macromers for Chondrocyte Encapsulation. *Macromolecules* **2004**, *37*, 6726–6733. [[CrossRef](#)]
16. Tan, B.; Gan, S.; Wang, X.; Liu, W.; Li, X. Applications of 3D Bioprinting in Tissue Engineering: Advantages, Deficiencies, Improvements, and Future Perspectives. *J. Mater. Chem. B* **2021**, *9*, 5385–5413. [[CrossRef](#)]
17. Huang, J.; Xiong, J.; Wang, D.; Zhang, J.; Yang, L.; Sun, S.; Liang, Y. 3D Bioprinting of Hydrogels for Cartilage Tissue Engineering. *Gels* **2021**, *7*, 144. [[CrossRef](#)]
18. Hospodiuk, M.; Dey, M.; Sosnoski, D.; Ozbolat, I.T. The Bioink: A Comprehensive Review on Bioprintable Materials. *Biotechnol. Adv.* **2017**, *35*, 217–239. [[CrossRef](#)]
19. Zhao, X.; Hu, D.A.; Wu, D.; He, F.; Wang, H.; Huang, L.; Shi, D.; Liu, Q.; Ni, N.; Pakvasa, M.; et al. Applications of Biocompatible Scaffold Materials in Stem Cell-Based Cartilage Tissue Engineering. *Front. Bioeng. Biotechnol.* **2021**, *9*, 603444. [[CrossRef](#)]
20. Decarli, M.C.; Seijas-Gamardo, A.; Morgan, F.L.C.; Wieringa, P.; Baker, M.B.; Silva, J.V.L.; Moraes, Â.M.; Moroni, L.; Mota, C. Bioprinting of Stem Cell Spheroids Followed by Post-Printing Chondrogenic Differentiation for Cartilage Tissue Engineering. *Adv. Healthc. Mater.* **2023**, *12*, e2203021. [[CrossRef](#)]
21. Kronemberger, G.S.; Matsui, R.A.M.; Miranda, G.A.S.C.; Granjeiro, J.M.; Baptista, L.S. Cartilage and Bone Tissue Engineering Using Adipose Stromal/Stem Cells Spheroids as Building Blocks. *World J. Stem Cells* **2020**, *12*, 110–122. [[CrossRef](#)] [[PubMed](#)]
22. Veenendaal, L.; Longoni, A.; Hooper, G.J.; Lim, K.S.; Woodfield, T.B.F.; Lindberg, G.C.J. 3D-Bioassembly of VH-Spheroids for Cartilage Regeneration: In Vitro Evaluation of Chondrogenesis, Fusion and Lateral Integration. *Adv. Mater. Interfaces* **2022**, *9*, 2200882. [[CrossRef](#)]
23. Schrobback, K.; Klein, T.J.; Crawford, R.; Upton, Z.; Malda, J.; Leavesley, D.I. Effects of Oxygen and Culture System on In Vitro Propagation and Redifferentiation of Osteoarthritic Human Articular Chondrocytes. *Cell Tissue Res.* **2012**, *347*, 649–663. [[CrossRef](#)] [[PubMed](#)]
24. Akkouch, A.; Yu, Y.; Ozbolat, I.T. Microfabrication of Scaffold-Free Tissue Strands for Three-Dimensional Tissue Engineering. *Biofabrication* **2015**, *7*, d031002. [[CrossRef](#)] [[PubMed](#)]
25. Roseti, L.; Cavallo, C.; Desando, G.; Parisi, V.; Petretta, M.; Bartolotti, I.; Grigolo, B. Three-Dimensional Bioprinting of Cartilage by the Use of Stem Cells: A Strategy to Improve Regeneration. *Materials* **2018**, *11*, 1749. [[CrossRef](#)]
26. Schuurman, W.; Klein, T.J.; Dhert, W.J.A.; van Weeren, P.R.; Huttmacher, D.W.; Malda, J. Cartilage Regeneration Using Zonal Chondrocyte Subpopulations: A Promising Approach or an Overcomplicated Strategy? *J. Tissue Eng. Regen. Med.* **2015**, *9*, 669–678. [[CrossRef](#)]
27. Klein, T.J.; Rizzi, S.C.; Reichert, J.C.; Georgi, N.; Malda, J.; Schuurman, W.; Crawford, R.W.; Huttmacher, D.W. Strategies for Zonal Cartilage Repair Using Hydrogels. *Macromol. Biosci.* **2009**, *9*, 1049–1058. [[CrossRef](#)]
28. Di Bella, C.; Duchi, S.; O'Connell, C.D.; Blanchard, R.; Augustine, C.; Yue, Z.; Thompson, F.; Richards, C.; Beirne, S.; Onofrillo, C.; et al. In Situ Handheld Three-dimensional Bioprinting for Cartilage Regeneration. *J. Tissue Eng. Regen. Med.* **2018**, *12*, 611–621. [[CrossRef](#)]
29. Rhee, S.; Puetzer, J.L.; Mason, B.N.; Reinhart-King, C.A.; Bonassar, L.J. 3D Bioprinting of Spatially Heterogeneous Collagen Constructs for Cartilage Tissue Engineering. *ACS Biomater. Sci. Eng.* **2016**, *2*, 1800–1805. [[CrossRef](#)]
30. Luo, Y.; Wei, X.; Huang, P. 3D Bioprinting of Hydrogel-based Biomimetic Microenvironments. *J. Biomed. Mater. Res. Part B Appl. Biomater.* **2019**, *107*, 1695–1705. [[CrossRef](#)]

31. Jang, J.; Park, J.Y.; Gao, G.; Cho, D.W. Biomaterials-Based 3D Cell Printing for next-Generation Therapeutics and Diagnostics. *Biomaterials* **2018**, *156*, 88–106. [[CrossRef](#)] [[PubMed](#)]
32. Mouser, V.H.M.; Abbadessa, A.; Levato, R.; Hennink, W.E.; Vermonden, T.; Gawlitta, D.; Malda, J. Development of a Thermosensitive HAMA-Containing Bio-Ink for the Fabrication of Composite Cartilage Repair Constructs. *Biofabrication* **2017**, *9*, 015026. [[CrossRef](#)] [[PubMed](#)]
33. Jessop, Z.M.; Gao, N.; Manivannan, S.; Al-Sabah, A.; Whitaker, I.S. 3D Bioprinting Cartilage. In *3D Bioprinting for Reconstructive Surgery: Techniques and Applications*; Elsevier Inc.: Amsterdam, The Netherlands, 2018; pp. 277–304, ISBN 9780081012161.
34. Williams, S.K.; Hoying, J.B. Bioinks for Bioprinting. In *Bioprinting in Regenerative Medicine*; Springer: Cham, Switzerland, 2015; pp. 1–31, ISBN 9783319213866.
35. Yang, Z.; Yi, P.; Liu, Z.; Zhang, W.; Mei, L.; Feng, C.; Tu, C.; Li, Z. Stem Cell-Laden Hydrogel-Based 3D Bioprinting for Bone and Cartilage Tissue Engineering. *Front. Bioeng. Biotechnol.* **2022**, *10*, 865770. [[CrossRef](#)] [[PubMed](#)]
36. Schuurman, W.; Khristov, V.; Pot, M.W.; Van Weeren, P.R.; Dhert, W.J.A.; Malda, J. Bioprinting of Hybrid Tissue Constructs with Tailorable Mechanical Properties. *Biofabrication* **2011**, *3*, 021001. [[CrossRef](#)] [[PubMed](#)]
37. Holmes, B.; Zhu, W.; Li, J.; Lee, J.D.; Zhang, L.G. Development of Novel Three-Dimensional Printed Scaffolds for Osteochondral Regeneration. *Tissue Eng. Part A* **2015**, *21*, 403–415. [[CrossRef](#)]
38. Pati, F.; Jang, J.; Ha, D.H.; Won Kim, S.; Rhie, J.W.; Shim, J.H.; Kim, D.H.; Cho, D.W. Printing Three-Dimensional Tissue Analogues with Decellularized Extracellular Matrix Bioink. *Nat. Commun.* **2014**, *5*, 935. [[CrossRef](#)]
39. Ren, X.; Wang, F.; Chen, C.; Gong, X.; Yin, L.; Yang, L. Engineering Zonal Cartilage through Bioprinting Collagen Type II Hydrogel Constructs with Biomimetic Chondrocyte Density Gradient. *BMC Musculoskelet. Disord.* **2016**, *17*, 301. [[CrossRef](#)]
40. Kundu, J.; Shim, J.H.; Jang, J.; Kim, S.W.; Cho, D.W. An Additive Manufacturing-Based PCL-Alginate-Chondrocyte Bioprinted Scaffold for Cartilage Tissue Engineering. *J. Tissue Eng. Regen. Med.* **2015**, *9*, 1286–1297. [[CrossRef](#)]
41. Carrow, J.K.; Keratitayanan, P.; Jaiswal, M.K.; Lokhande, G.; Gaharwar, A.K. Polymers for Bioprinting. In *Essentials of 3D Biofabrication and Translation*; Elsevier Inc.: Amsterdam, The Netherlands, 2015; pp. 229–248, ISBN 9780128010150.
42. Izadifar, Z.; Chang, T.; Kulyk, W.; Chen, X.; Eames, B.F. Analyzing Biological Performance of 3D-Printed, Cell-Impregnated Hybrid Constructs for Cartilage Tissue Engineering. *Tissue Eng. Part C Methods* **2016**, *22*, 173–188. [[CrossRef](#)]
43. Munaz, A.; Vadivelu, R.K.; John, J.S.; Barton, M.; Kamble, H.; Nguyen, N.T. Three-Dimensional Printing of Biological Matters. *J. Sci. Adv. Mater. Devices* **2016**, *1*, 1–17. [[CrossRef](#)]
44. Xu, B.; Ye, J.; Yuan, F.Z.; Zhang, J.Y.; Chen, Y.R.; Fan, B.S.; Jiang, D.; Jiang, W.B.; Wang, X.; Yu, J.K. Advances of Stem Cell-Laden Hydrogels With Biomimetic Microenvironment for Osteochondral Repair. *Front. Bioeng. Biotechnol.* **2020**, *8*, 247. [[CrossRef](#)] [[PubMed](#)]
45. McGivern, S.; Boutouil, H.; Al-Kharusi, G.; Little, S.; Dunne, N.J.; Levingstone, T.J. Translational Application of 3D Bioprinting for Cartilage Tissue Engineering. *Bioengineering* **2021**, *8*, 144. [[CrossRef](#)]
46. Liu, N.; Zhang, X.; Guo, Q.; Wu, T.; Wang, Y. 3D Bioprinted Scaffolds for Tissue Repair and Regeneration. *Front. Mater.* **2022**, *9*, 25321. [[CrossRef](#)]
47. Cui, X.; Gao, G.; Yonezawa, T.; Dai, G. Human Cartilage Tissue Fabrication Using Three-Dimensional Inkjet Printing Technology. *J. Vis. Exp.* **2014**, *8*, 51294.
48. Xu, T.; Binder, K.W.; Albanna, M.Z.; Dice, D.; Zhao, W.; Yoo, J.J.; Atala, A. Hybrid Printing of Mechanically and Biologically Improved Constructs for Cartilage Tissue Engineering Applications. *Biofabrication* **2013**, *5*, 015001. [[CrossRef](#)] [[PubMed](#)]
49. Gruene, M.; Deiwick, A.; Koch, L.; Schlie, S.; Unger, C.; Hofmann, N.; Bernemann, I.; Glasmacher, B.; Chichkov, B. Laser Printing of Stem Cells for Biofabrication of Scaffold-Free Autologous Grafts. *Tissue Eng. Part C Methods* **2010**, *17*, 9–87. [[CrossRef](#)]
50. Medvedeva, E.V.; Grebenik, E.A.; Gornostaeva, S.N.; Telpuhov, V.I.; Lychagin, A.V.; Timashev, P.S.; Chagin, A.S. Repair of Damaged Articular Cartilage: Current Approaches and Future Directions. *Int. J. Mol. Sci.* **2018**, *19*, 2366. [[CrossRef](#)]
51. Derakhshanfar, S.; Mbeleck, R.; Xu, K.; Zhang, X.; Zhong, W.; Xing, M. 3D Bioprinting for Biomedical Devices and Tissue Engineering: A Review of Recent Trends and Advances. *Bioact. Mater.* **2018**, *3*, 4–156. [[CrossRef](#)]
52. Bauer, C.; Moser, L.B.; Kern, D.; Jeyakumar, V.; Nehrer, S. The Combination of Glucocorticoids and Hyaluronic Acid Enhances Efficacy in IL-1 β /IL-17-Treated Bovine Osteochondral Grafts Compared with Individual Application. *Int. J. Mol. Sci.* **2023**, *24*, 14338. [[CrossRef](#)]
53. Bauer, C.; Moser, L.B.; Jeyakumar, V.; Niculescu-Morzsza, E.; Kern, D.; Nehrer, S. Increased Chondroprotective Effect of Combining Hyaluronic Acid with a Glucocorticoid Compared to Separate Administration on Cytokine-Treated Osteoarthritic Chondrocytes in a 2D Culture. *Biomedicines* **2022**, *10*, 733. [[CrossRef](#)]
54. Akmal, M.; Singh, A.; Anand, A.; Kesani, A.; Aslam, N.; Goodship, A.; Bentley, G. The Effects of Hyaluronic Acid on Articular Chondrocytes. *J. Bone Jt. Surg. Ser. B* **2005**, *87*, 1143–1149. [[CrossRef](#)] [[PubMed](#)]
55. López-Ruiz, E.; Jiménez, G.; Álvarez de Cienfuegos, L.; Antic, C.; Sabata, R.; Marchal, J.A.; Gálvez-Martín, P. Advances of Hyaluronic Acid in Stem Cell Therapy and Tissue Engineering, Including Current Clinical Trials. *Eur. Cell Mater.* **2019**, *37*, 186–213. [[CrossRef](#)] [[PubMed](#)]
56. Knudson, C.B. Hyaluronan and CD44: Strategic Players for Cell-Matrix Interactions during Chondrogenesis and Matrix Assembly. *Birth Defects Res. Part C Embryo Today Rev.* **2003**, *69*, 174–196. [[CrossRef](#)] [[PubMed](#)]

57. Matsiko, A.; Levingstone, T.J.; O'Brien, F.J.; Gleeson, J.P. Addition of Hyaluronic Acid Improves Cellular Infiltration and Promotes Early-Stage Chondrogenesis in a Collagen-Based Scaffold for Cartilage Tissue Engineering. *J. Mech. Behav. Biomed. Mater.* **2012**, *11*, 41–52. [[CrossRef](#)] [[PubMed](#)]
58. Muran, A.C.; Schaffler, B.C.; Wong, A.; Neufeld, E.; Swami, P.; Pianka, M.; Grande, D. Effect of Increasing Hyaluronic Acid Content in Collagen Scaffolds on the Maintenance of Chondrogenic Phenotype in Chondrocytes and Mesenchymal Stem Cells. *J. Cartil. Jt. Preserv.* **2023**, *3*, 41–52. [[CrossRef](#)]
59. Chung, C.; Mesa, J.; Randolph, M.A.; Yaremchuk, M.; Burdick, J.A. Influence of Gel Properties on Neocartilage Formation by Auricular Chondrocytes Photoencapsulated in Hyaluronic Acid Networks. *J. Biomed. Mater. Res. Part A* **2006**, *77*, 518–525. [[CrossRef](#)]
60. Park, H.; Lee, K.Y. Cartilage Regeneration Using Biodegradable Oxidized Alginate/Hyaluronate Hydrogels. *J. Biomed. Biotechnol.* **2012**, *2012*, 4519–4525. [[CrossRef](#)]
61. Nava, M.M.; Raimondi, M.T.; Pietrabissa, R. Controlling Self-Renewal and Differentiation of Stem Cells via Mechanical Cues. *J. Biomed. Biotechnol.* **2012**, *2012*, 797410. [[CrossRef](#)]
62. Guvendiren, M.; Lu, H.D.; Burdick, J.A. Shear-Thinning Hydrogels for Biomedical Applications. *Soft Matter* **2012**, *8*, 260–272. [[CrossRef](#)]
63. Acharya, C.; Adesida, A.; Zajac, P.; Mumme, M.; Riesle, J.; Martin, I.; Barbero, A. Enhanced Chondrocyte Proliferation and Mesenchymal Stromal Cells Chondrogenesis in Coculture Pellets Mediate Improved Cartilage Formation. *J. Cell Physiol.* **2012**, *227*, 88–97. [[CrossRef](#)]
64. Suwannaloet, W.; Laupattarakasem, W.; Sukon, P.; Ong-Chai, S.; Laupattarakasem, P. Combined Effect of Subchondral Drilling and Hyaluronic Acid with/without Diacerein in Full-Thickness Articular Cartilage Lesion in Rabbits. *Sci. World J.* **2012**, *2012*, 310745. [[CrossRef](#)] [[PubMed](#)]
65. Katoh, S.; Yoshioka, H.; Senthilkumar, R.; Preethy, S.; Abraham, S.J.K. Enhanced Expression of Hyaluronic Acid in Osteoarthritis-Affected Knee-Cartilage Chondrocytes during Three-Dimensional In Vitro Culture in a Hyaluronic-Acid-Retaining Polymer Scaffold. *Knee* **2021**, *29*, 365–373. [[CrossRef](#)] [[PubMed](#)]
66. Ziadlou, R.; Rotman, S.; Teuschl, A.; Salzer, E.; Barbero, A.; Martin, I.; Alini, M.; Eglin, D.; Grad, S. Optimization of Hyaluronic Acid-Tyramine/Silk-Fibroin Composite Hydrogels for Cartilage Tissue Engineering and Delivery of Anti-Inflammatory and Anabolic Drugs. *Mater. Sci. Eng. C* **2021**, *120*, 111701. [[CrossRef](#)] [[PubMed](#)]
67. Gopinathan, J.; Noh, I. Recent Trends in Bioinks for 3D Printing. *Biomater. Res.* **2018**, *22*, 11. [[CrossRef](#)] [[PubMed](#)]
68. Khoeini, R.; Nosrati, H.; Akbarzadeh, A.; Eftekhari, A.; Kavetsky, T.; Khalilov, R.; Ahmadian, E.; Nasibova, A.; Datta, P.; Roshangar, L.; et al. Natural and Synthetic Bioinks for 3D Bioprinting. *Adv. NanoBiomed Res.* **2021**, *8*, 2000097. [[CrossRef](#)]
69. Ozbolat, I.T.; Hospodiuk, M. Current Advances and Future Perspectives in Extrusion-Based Bioprinting. *Biomaterials* **2016**, *76*, 21–343. [[CrossRef](#)]
70. Antich, C.; de Vicente, J.; Jiménez, G.; Chocarro, C.; Carrillo, E.; Montañez, E.; Gálvez-Martín, P.; Marchal, J.A. Bio-Inspired Hydrogel Composed of Hyaluronic Acid and Alginate as a Potential Bioink for 3D Bioprinting of Articular Cartilage Engineering Constructs. *Acta Biomater.* **2020**, *106*, 114–123. [[CrossRef](#)]
71. Poldervaart, M.T.; Goversen, B.; De Ruijter, M.; Abbadessa, A.; Melchels, F.P.W.; Öner, F.C.; Dhert, W.J.A.; Vermonden, T.; Alblas, J. 3D Bioprinting of Methacrylated Hyaluronic Acid (MeHA) Hydrogel with Intrinsic Osteogenicity. *PLoS ONE* **2017**, *12*, e0177628. [[CrossRef](#)]
72. Petta, D.; Armiento, A.R.; Grijpma, D.; Alini, M.; Eglin, D.; D'Este, M. 3D Bioprinting of a Hyaluronan Bioink through Enzymatic and Visible Light-Crosslinking. *Biofabrication* **2018**, *10*, 044104. [[CrossRef](#)]
73. Xu, J.; Wang, W.; Ludeman, M.; Cheng, K.; Hayami, T.; Lotz, J.C.; Kapila, S. Chondrogenic Differentiation of Human Mesenchymal Stem Cells in Three-Dimensional Alginate Gels. *Tissue Eng. Part A* **2008**, *14*, 667–680. [[CrossRef](#)]
74. Wang, W.Z.; Yao, X.D.; Huang, X.J.; Li, J.Q.; Xu, H. Effects of TGF-β1 and Alginate on the Differentiation of Rabbit Bone Marrow-Derived Mesenchymal Stem Cells into a Chondrocyte Cell Lineage. *Exp. Ther. Med.* **2015**, *10*, 995–1002. [[CrossRef](#)] [[PubMed](#)]
75. Reppel, L.; Schiavi, J.; Charif, N.; Leger, L.; Yu, H.; Pinzano, A.; Henrionnet, C.; Stoltz, J.F.; Bensoussan, D.; Huselstein, C. Chondrogenic Induction of Mesenchymal Stromal/Stem Cells from Wharton's Jelly Embedded in Alginate Hydrogel and without Added Growth Factor: An Alternative Stem Cell Source for Cartilage Tissue Engineering. *Stem Cell Res. Ther.* **2015**, *6*, 260. [[CrossRef](#)] [[PubMed](#)]
76. Park, J.Y.; Choi, Y.-J.; Shim, J.-H.; Park, J.H.; Cho, D.-W. Development of a 3D Cell Printed Structure as an Alternative to Autologous Cartilage for Auricular Reconstruction. *J. Biomed. Mater. Res. Part B Appl. Biomater.* **2017**, *105*, 1016–1028. [[CrossRef](#)] [[PubMed](#)]
77. Singhvi, M.S.; Zinjarde, S.S.; Gokhale, D.V. Polylactic Acid: Synthesis and Biomedical Applications. *J. Appl. Microbiol.* **2019**, *127*, 1612–1626. [[CrossRef](#)] [[PubMed](#)]
78. DeStefano, V.; Khan, S.; Tabada, A. Applications of PLA in Modern Medicine. *Eng. Regen.* **2020**, *1*, 76–87. [[CrossRef](#)]
79. Wang, X.; Li, G.; Liu, Y.; Yu, W.; Sun, Q. Biocompatibility of Biological Material Polylactic Acid with Stem Cells from Human Exfoliated Deciduous Teeth. *Biomed. Rep.* **2017**, *6*, 519–524. [[CrossRef](#)]
80. Feng, P.; Jia, J.; Liu, M.; Peng, S.; Zhao, Z.; Shuai, C. Degradation Mechanisms and Acceleration Strategies of Poly(lactic acid) Scaffold for Bone Regeneration. *Mater. Des.* **2021**, *210*, 110066. [[CrossRef](#)]

81. Vuornos, K.; Björninen, M.; Talvitie, E.; Paakinaho, K.; Kellomäki, M.; Huhtala, H.; Miettinen, S.; Seppänen-Kaijansinkko, R.; Haimi, S. Human Adipose Stem Cells Differentiated on Braided Polylactide Scaffolds Is a Potential Approach for Tendon Tissue Engineering. *Tissue Eng. Part A* **2016**, *22*, 513–523. [[CrossRef](#)]
82. Salerno, A.; Guarino, V.; Oliviero, O.; Ambrosio, L.; Domingo, C. Bio-Safe Processing of Polylactic-co-caprolactone and Polylactic Acid Blends to Fabricate Fibrous Porous Scaffolds for In Vitro Mesenchymal Stem Cells Adhesion and Proliferation. *Mater. Sci. Eng. C* **2016**, *63*, 12–21. [[CrossRef](#)]
83. Sudwilai, T.; Ng, J.J.; Boonkrai, C.; Israsena, N.; Chuangchote, S.; Supaphol, P. Polypyrrole-Coated Electrospun Poly(lactic acid) Fibrous Scaffold: Effects of Coating on Electrical Conductivity and Neural Cell Growth. *J. Biomater. Sci. Polym. Ed.* **2014**, *25*, 1240–1252. [[CrossRef](#)]
84. Gupta, B.; Revagade, N.; Hilborn, J. Poly(lactic acid) Fiber: An Overview. *Prog. Polym. Sci.* **2007**, *32*, 455–482. [[CrossRef](#)]
85. Madhavan Nampoothiri, K.; Nair, N.R.; John, R.P. An Overview of the Recent Developments in Polylactide (PLA) Research. *Bioresour. Technol.* **2010**, *101*, 8493–8501. [[CrossRef](#)] [[PubMed](#)]
86. Yamane, H.; Sasai, K. Effect of the Addition of Poly(D-lactic acid) on the Thermal Property of Poly(L-lactic acid). *Polymer* **2003**, *44*, 2569–2575. [[CrossRef](#)]
87. Emami, F.; Mostafavi Yazdi, S.J.; Na, D.H. Poly(lactic acid)/Poly(lactic-co-glycolic acid) Particulate Carriers for Pulmonary Drug Delivery. *J. Pharm. Investig.* **2019**, *49*, 427–442. [[CrossRef](#)]
88. Youssef, A.; Hollister, S.J.; Dalton, P.D. Additive Manufacturing of Polymer Melts for Implantable Medical Devices and Scaffolds. *Biofabrication* **2017**, *9*, 012002. [[CrossRef](#)]
89. Sekiya, I.; Vuoristo, J.T.; Larson, B.L.; Prockop, D.J. In Vitro Cartilage Formation by Human Adult Stem Cells from Bone Marrow Stroma Defines the Sequence of Cellular and Molecular Events during Chondrogenesis. *Proc. Natl. Acad. Sci. USA* **2002**, *99*, 4397–4402. [[CrossRef](#)]
90. Ma, H.L.; Hung, S.C.; Lin, S.Y.; Chen, Y.L.; Lo, W.H. Chondrogenesis of Human Mesenchymal Stem Cells Encapsulated in Alginate Beads. *J. Biomed. Mater. Res. Part A* **2003**, *64*, 273–281. [[CrossRef](#)]
91. Ma, H.-L.; Chen, T.-H.; Low-Tone Ho, L.; Hung, S.-C. Neocartilage from Human Mesenchymal Stem Cells in Alginate: Implied Timing of Transplantation. *J. Biomed. Mater. Res. Part A* **2005**, *74*, 439–446. [[CrossRef](#)]
92. Guadix, J.A.; Zugaza, J.L.; Gálvez-Martín, P. Características, Aplicaciones y Perspectivas de Las Células Madre Mesenquimales En Terapia Celular. *Med. Clin.* **2017**, *148*, 408–414. [[CrossRef](#)]
93. Larsen, S.; Lewis, I.D. Potential Therapeutic Applications of Mesenchymal Stromal Cells. *Pathology* **2011**, *43*, 592–604. [[CrossRef](#)]
94. Yi, T.; Song, S.U. Immunomodulatory Properties of Mesenchymal Stem Cells and Their Therapeutic Applications. *Arch. Pharm. Res.* **2012**, *35*, 213–221. [[CrossRef](#)] [[PubMed](#)]
95. Alcaide-Ruggiero, L.; Molina-Hernández, V.; Granados, M.M.; Domínguez, J.M. Main and Minor Types of Collagens in the Articular Cartilage: The Role of Collagens in Repair Tissue Evaluation in Chondral Defects. *Int. J. Mol. Sci.* **2021**, *22*, 13329. [[CrossRef](#)] [[PubMed](#)]
96. Costa, E.; González-García, C.; Gómez Ribelles, J.L.; Salmerón-Sánchez, M. Maintenance of Chondrocyte Phenotype during Expansion on PLLA Microtopographies. *J. Tissue Eng.* **2018**, *9*, 2041731418789829. [[CrossRef](#)] [[PubMed](#)]
97. Gimble, J.M.; Guilak, F. Adipose-Derived Adult Stem Cells: Isolation, Characterization, and Differentiation Potential. *Cytotherapy* **2003**, *5*, 362–369. [[CrossRef](#)]
98. Jeon, Y.J.; Kim, J.; Cho, J.H.; Chung, H.M.; Chae, J. II Comparative Analysis of Human Mesenchymal Stem Cells Derived from Bone Marrow, Placenta, and Adipose Tissue as Sources of Cell Therapy. *J. Cell Biochem.* **2016**, *117*, 1112–1125. [[CrossRef](#)]
99. English, A.; Jones, E.A.; Corscadden, D.; Henshaw, K.; Chapman, T.; Emery, P.; McGonagle, D. A Comparative Assessment of Cartilage and Joint Fat Pad as a Potential Source of Cells for Autologous Therapy Development in Knee Osteoarthritis. *Rheumatology* **2007**, *46*, 1676–1683. [[CrossRef](#)]
100. Buckley, C.T.; Vinardell, T.; Thorpe, S.D.; Haugh, M.G.; Jones, E.; McGonagle, D.; Kelly, D.J. Functional Properties of Cartilaginous Tissues Engineered from Infrapatellar Fat Pad-Derived Mesenchymal Stem Cells. *J. Biomech.* **2010**, *43*, 920–926. [[CrossRef](#)]
101. Shie, M.Y.; Chang, W.C.; Wei, L.J.; Huang, Y.H.; Chen, C.H.; Shih, C.T.; Chen, Y.W.; Shen, Y.F. 3D Printing of Cytocompatible Water-Based Light-Cured Polyurethane with Hyaluronic Acid for Cartilage Tissue Engineering Applications. *Materials* **2017**, *10*, 136. [[CrossRef](#)]
102. Rencsok, M.; Stichler, S.; Böck, T.; Paxton, N.; Bertlein, S.; Levato, R.; Schill, V. Double Printing of Hyaluronic Acid/Poly(glycidol) Hybrid Hydrogels with Poly(ϵ -caprolactone) for MSC Chondrogenesis. *Biofabrication* **2017**, *9*, 044108.
103. Levett, P.A.; Hutmacher, D.W.; Malda, J.; Klein, T.J. Hyaluronic Acid Enhances the Mechanical Properties of Tissue-Engineered Cartilage Constructs. *PLoS ONE* **2014**, *9*, 0113216. [[CrossRef](#)]
104. Unterman, S.A.; Gibson, M.; Lee, J.H.; Crist, J.; Chansakul, T.; Yang, E.C.; Elisseeff, J.H. Hyaluronic Acid-Binding Scaffold for Articular Cartilage Repair. *Tissue Eng. Part A* **2012**, *18*, 497–506. [[CrossRef](#)] [[PubMed](#)]
105. Lafuente-Merchan, M.; Ruiz-Alonso, S.; Espona-Noguera, A.; Galvez-Martin, P.; López-Ruiz, E.; Marchal, J.A.; López-Donaire, M.L.; Zabala, A.; Ciriza, J.; Saenz-del-Burgo, L.; et al. Development, Characterization and Sterilisation of Nanocellulose-Alginate-(Hyaluronic Acid)—Bioinks and 3D Bioprinted Scaffolds for Tissue Engineering. *Mater. Sci. Eng. C* **2021**, *126*, 112160. [[CrossRef](#)]

106. Jeong, J.Y.; Park, S.H.; Shin, J.W.; Kang, Y.G.; Han, K.H.; Shin, J.W. Effects of Intermittent Hydrostatic Pressure Magnitude on the Chondrogenesis of MSCs without Biochemical Agents under 3D Co-Culture. *J. Mater. Sci. Mater. Med.* **2012**, *23*, 2773–2781. [[CrossRef](#)] [[PubMed](#)]
107. Loh, Q.L.; Choong, C. Three-Dimensional Scaffolds for Tissue Engineering Applications: Role of Porosity and Pore Size. *Tissue Eng. Part B Rev.* **2013**, *19*, 485–502. [[CrossRef](#)] [[PubMed](#)]
108. Kuo, C.K.; Ma, P.X. Maintaining Dimensions and Mechanical Properties of Ionically Crosslinked Alginate Hydrogel Scaffolds In Vitro. *J. Biomed. Mater. Res. Part A* **2008**, *84*, 99–107. [[CrossRef](#)] [[PubMed](#)]
109. López-Ruiz, E.; Jiménez, G.; Kwiatkowski, W.; Montañez, E.; Arrebola, F.; Carrillo, E.; Choe, S.; Marchal, J.A.; Perán, M. Impact of TGF- β Family-Related Growth Factors on Chondrogenic Differentiation of Adipose-Derived Stem Cells Isolated from Lipoaspirates and Infrapatellar Fat Pads of Osteoarthritic Patients. *Eur. Cells Mater.* **2018**, *35*, 209–224. [[CrossRef](#)] [[PubMed](#)]
110. Mallandrich, M.; Fernández-Campos, F.; Clares, B.; Halbaut, L.; Alonso, C.; Coderch, L.; Garduño-Ramírez, M.L.; Andrade, B.; del Pozo, A.; Lane, M.E.; et al. Developing Transdermal Applications of Ketorolac Tromethamine Entrapped in Stimuli Sensitive Block Copolymer Hydrogels. *Pharm. Res.* **2017**, *34*, 1728–1740. [[CrossRef](#)]
111. Shahini, A.; Yazdimamaghani, M.; Walker, K.J.; Eastman, M.A.; Hatami-Marbini, H.; Smith, B.J.; Ricci, J.L.; Madihally, S.V.; Vashae, D.; Tayebi, L. 3D Conductive Nanocomposite Scaffold for Bone Tissue Engineering. *Int. J. Nanomed.* **2013**, *9*, 167–181.
112. Cui, N.; Qian, J.; Liu, T.; Zhao, N.; Wang, H. Hyaluronic Acid Hydrogel Scaffolds with a Triple Degradation Behavior for Bone Tissue Engineering. *Carbohydr. Polym.* **2015**, *126*, 192–198. [[CrossRef](#)]
113. Felfel, R.M.; Poczka, L.; Gimeno-Fabra, M.; Milde, T.; Hildebrand, G.; Ahmed, I.; Scotchford, C.; Sottile, V.; Grant, D.M.; Liefelth, K. In Vitro Degradation and Mechanical Properties of PLA-PCL Copolymer Unit Cell Scaffolds Generated by Two-Photon Polymerization. *Biomed. Mater.* **2016**, *11*, 015011. [[CrossRef](#)]
114. Dong, L.; Wang, S.J.; Zhao, X.R.; Zhu, Y.F.; Yu, J.K. 3D-Printed Poly(ϵ -caprolactone) Scaffold Integrated with Cell-Laden Chitosan Hydrogels for Bone Tissue Engineering. *Sci. Rep.* **2017**, *7*, 4–12. [[CrossRef](#)] [[PubMed](#)]
115. Cipollaro, L.; Ciardulli, M.C.; Della Porta, G.; Peretti, G.M.; Maffulli, N. Biomechanical Issues of Tissue-Engineered Constructs for Articular Cartilage Regeneration: In Vitro and In Vivo Approaches. *Br. Med. Bull.* **2019**, *132*, 53–80. [[CrossRef](#)] [[PubMed](#)]
116. Gungor-Ozkerim, P.S.; Inci, I.; Zhang, Y.S.; Khademhosseini, A.; Dokmeci, M.R. Bioinks for 3D Bioprinting: An Overview. *Biomater. Sci.* **2018**, *6*, 915–946. [[CrossRef](#)] [[PubMed](#)]
117. Groll, J.; Burdick, J.A.; Cho, D.W.; Derby, B.; Gelinsky, M.; Heilshorn, S.C.; Jüngst, T.; Malda, J.; Mironov, V.A.; Nakayama, K.; et al. A Definition of Bioinks and Their Distinction from Biomaterial Inks. *Biofabrication* **2019**, *11*, 13001. [[CrossRef](#)] [[PubMed](#)]
118. Li, Y.; Liu, Y.; Xun, X.; Zhang, W.; Xu, Y.; Gu, D. Three-Dimensional Porous Scaffolds with Biomimetic Microarchitecture and Bioactivity for Cartilage Tissue Engineering. *ACS Appl. Mater. Interfaces* **2019**, *11*, 359–36370. [[CrossRef](#)]
119. O'Brien, F.J. Biomaterials & Scaffolds for Tissue Engineering. *Mater. Today* **2011**, *14*, 88–95.
120. Liang, K. Tissue Bioprinting: Promise and Challenges. *Bioengineering* **2023**, *10*, 1400. [[CrossRef](#)]
121. Vijayavenkataraman, S. 3D Bioprinting: Challenges in Commercialization and Clinical Translation. *J. 3D Print. Med.* **2023**, *7*, 3DP8. [[CrossRef](#)]
122. Kim, K.; Yoon, D.M.; Mikos, A.; Kasper, F.K. Harnessing Cell-Biomaterial Interactions for Osteochondral Tissue Regeneration. *Adv. Biochem. Eng. Biotechnol.* **2012**, *126*, 67–104.
123. Axpe, E.; Oyen, M. Applications of Alginate-Based Bioinks in 3D Bioprinting. *Int. J. Mol. Sci.* **2016**, *17*, 1976. [[CrossRef](#)]
124. Song, Y.; Du, H.; Dai, C.; Zhang, L.; Li, S.; Hunter, D.J.; Lu, L.; Bao, C. Human Adipose-Derived Mesenchymal Stem Cells for Osteoarthritis: A Pilot Study with Long-Term Follow-up and Repeated Injections. *Regen. Med.* **2018**, *13*, 295–307. [[CrossRef](#)] [[PubMed](#)]
125. Dominici, M.; Le Blanc, K.; Mueller, I.; Slaper-Cortenbach, I.; Marini, F.C.; Krause, D.S.; Deans, R.J.; Keating, A.; Prockop, D.J.; Horwitz, E.M. Minimal Criteria for Defining Multipotent Mesenchymal Stromal Cells. The International Society for Cellular Therapy Position Statement. *Cytotherapy* **2006**, *8*, 315–317. [[CrossRef](#)] [[PubMed](#)]
126. Nery, A.A.; Nascimento, I.C.; Glaser, T.; Bassaneze, V.; Krieger, J.E.; Ulrich, H. Human Mesenchymal Stem Cells: From Immunophenotyping by Flow Cytometry to Clinical Applications. *Cytom. Part A* **2013**, *83*, 48–61. [[CrossRef](#)] [[PubMed](#)]
127. Kuo, J.W. *Practical Aspects of Hyaluronan-Based Medical Products*, 1st ed.; CRC Press: Boca Raton, FL, USA, 2005.
128. Abe, M.; Takahashi, M.; Nagano, A. The Effect of Hyaluronic Acid with Different Molecular Weights on Collagen Crosslink Synthesis in Cultured Chondrocytes Embedded in Collagen Gels. *J. Biomed. Mater. Res. A* **2005**, *75*, 494–499. [[CrossRef](#)] [[PubMed](#)]
129. Kawasaki, K.; Ochi, M.; Uchio, Y.; Adachi, N.; Matsusaki, M. Hyaluronic Acid Enhances Proliferation and Chondroitin Sulfate Synthesis in Cultured Chondrocytes Embedded in Collagen Gels. *J. Cell. Physiol.* **1999**, *179*, 142–148. [[CrossRef](#)]
130. Herlofsen, S.R.; Küchler, A.M.; Melvik, J.E.; Brinchmann, J.E. Chondrogenic Differentiation of Human Bone Marrow-Derived Mesenchymal Stem Cells in Self-Gelling Alginate Discs Reveals Novel Chondrogenic Signature Gene Clusters. *Tissue Eng. Part A* **2011**, *17*, 1003–1013. [[CrossRef](#)]
131. Burdick, J.A.; Chung, C. Influence of Three-Dimensional Hyaluronic Acid Microenvironments on Mesenchymal Stem Cell Chondrogenesis. *Tissue Eng. Part A* **2009**, *15*, 243–254.
132. Liu, Y.; Shu, X.Z.; Prestwich, G.D. Osteochondral Defect Repair with Autologous Bone Marrow-Derived Mesenchymal Stem Cells in an Injectable, in Situ, Cross-Linked Synthetic Extracellular Matrix. *Tissue Eng.* **2006**, *12*, 3405–3416. [[CrossRef](#)]
133. Solchaga, L.A.; Dennis, J.E.; Goldberg, V.M.; Caplan, A.I. Hyaluronic Acid-Based Polymers as Cell Carriers for Tissue-Engineered Repair of Bone and Cartilage. *J. Orthop. Res.* **1999**, *17*, 205–213. [[CrossRef](#)]

134. Shigley, C.; Trivedi, J.; Meghani, O.; Owens, B.D.; Jayasuriya, C.T. Suppressing Chondrocyte Hypertrophy to Build Better Cartilage. *Bioengineering* **2023**, *10*, 741. [[CrossRef](#)]
135. Xu, J.H.; Li, Z.H.; Hou, Y.D.; Fang, W.J. Potential Mechanisms Underlying the Runx2 Induced Osteogenesis of Bone Marrow Mesenchymal Stem Cells. *Am. J. Transl. Res.* **2015**, *7*, 2527–2535. [[PubMed](#)]
136. Hölzl, K.; Lin, S.; Tytgat, L.; Van Vlierberghe, S.; Gu, L.; Ovsianikov, A. Bioink Properties before, during and after 3D Bioprinting. *Biofabrication* **2016**, *8*, 032002. [[CrossRef](#)] [[PubMed](#)]
137. Lu, L.; Zhu, X.; Valenzuela, R.G.; Currier, B.L.; Yaszemski, M.J. Biodegradable Polymer Scaffolds for Cartilage Tissue Engineering. *Clin. Orthop. Relat. Res.* **2001**, *391*, S251–S270. [[CrossRef](#)] [[PubMed](#)]
138. Bharatham, H.; Masre, S.F.; Xien, L.H.; Ahmad, N. Evaluating Physical and Biological Characteristics of Glutaraldehyde (GA) Cross-Linked Nano-Biocomposite Bone Scaffold. *Sains Malays.* **2018**, *47*, 2557–2563. [[CrossRef](#)]
139. Bharatham, B.H.; Abu Bakar, M.Z.; Perimal, E.K.; Yusof, L.M.; Hamid, M. Development and Characterization of Novel Porous 3D Alginate-Cockle Shell Powder Nanobiocomposite Bone Scaffold. *Biomed. Res. Int.* **2014**, *2014*, 146723. [[CrossRef](#)]
140. Sanzana, E.S.; Navarro, M.; Ginebra, M.P.; Planell, J.A.; Ojeda, A.C.; Montecinos, H.A. Role of Porosity and Pore Architecture in the In Vivo Bone Regeneration Capacity of Biodegradable Glass Scaffolds. *J. Biomed. Mater. Res. Part A* **2014**, *102*, 1767–1773. [[CrossRef](#)]
141. Correia, C.R.; Moreira-Teixeira, L.S.; Moroni, L.; Reis, R.L.; Van Blitterswijk, C.A.; Karperien, M.; Mano, J.F. Chitosan Scaffolds Containing Hyaluronic Acid for Cartilage Tissue Engineering. *Tissue Eng. Part C Methods* **2011**, *17*, 17–30. [[CrossRef](#)]
142. Compañ, V.; Guzmán, J.; Riande, E. A Potentiostatic Study of Oxygen Transmissibility and Permeability through Hydrogel Membranes. *Biomaterials* **1998**, *19*, 139–145. [[CrossRef](#)]
143. Singh, D.; Tripathi, A.; Zo, S.M.; Singh, D.; Han, S.S. Synthesis of Composite Gelatin-Hyaluronic Acid-Alginate Porous Scaffold and Evaluation for In Vitro Stem Cell Growth and In Vivo Tissue Integration. *Colloids Surf. B Biointerfaces* **2014**, *116*, 502–509. [[CrossRef](#)]
144. Rasal, R.M.; Janorkar, A.V.; Hirt, D.E. Poly(lactic acid) Modifications. *Prog. Polym. Sci.* **2010**, *35*, 338–356. [[CrossRef](#)]
145. Cheng, C.H.; Shie, M.Y.; Lai, Y.H.; Foo, N.P.; Lee, M.J.; Yao, C.H. Fabrication of 3d Printed Poly(lactic acid)/Polycaprolactone Scaffolds Using Tgf-B1 for Promoting Bone Regeneration. *Polymers* **2021**, *13*, 731. [[CrossRef](#)] [[PubMed](#)]
146. Nazeer, M.A.; Onder, O.C.; Sevgili, I.; Yilgor, E.; Kavakli, I.H.; Yilgor, I. 3D Printed Poly(lactic acid) Scaffolds Modified with Chitosan and Hydroxyapatite for Bone Repair Applications. *Mater. Today Commun.* **2020**, *25*, 01515. [[CrossRef](#)]
147. Elsayy, M.A.; Kim, K.H.; Park, J.W.; Deep, A. Hydrolytic Degradation of Polylactic Acid (PLA) and Its Composites. *Renew. Sustain. Energy Rev.* **2017**, *79*, 346–1352. [[CrossRef](#)]
148. Lovald, S.T.; Khraishi, T.; Wagner, J.; Baack, B. Mechanical Design Optimization of Bioabsorbable Fixation Devices for Bone Fractures. *J. Craniofac. Surg.* **2009**, *20*, 389–398. [[CrossRef](#)] [[PubMed](#)]
149. Sun, J.; Tan, H. Alginate-Based Biomaterials for Regenerative Medicine Applications. *Materials* **2013**, *6*, 1285–1309. [[CrossRef](#)]
150. Savioli Lopes, M.; Jardini, A.L.; Maciel Filho, R. Poly(lactic acid) Production for Tissue Engineering Applications. *Procedia Eng.* **2012**, *42*, 1402–1413. [[CrossRef](#)]
151. Odelius, K.; Höglund, A.; Kumar, S.; Hakkarainen, M.; Ghosh, A.K.; Bhatnagar, N.; Albertsson, A.C. Porosity and Pore Size Regulate the Degradation Product Profile of Polylactide. *Biomacromolecules* **2011**, *12*, 250–1258. [[CrossRef](#)]
152. Ferreira, J.; Gloria, A.; Cometa, S.; Coelho, J.F.J.; Domingos, M. Effect of In Vitro Enzymatic Degradation on 3D Printed Poly(ϵ -caprolactone) Scaffolds: Morphological, Chemical and Mechanical Properties. *J. Appl. Biomater. Funct. Mater.* **2017**, *15*, e185–e195. [[CrossRef](#)]
153. Zhang, Q.; Jiang, Y.; Zhang, Y.; Ye, Z.; Tan, W.; Lang, M. Effect of Porosity on Long-Term Degradation of Poly(ϵ -caprolactone) Scaffolds and Their Cellular Response. *Polym. Degrad. Stab.* **2013**, *98*, 209–218. [[CrossRef](#)]
154. Chen, Y.M.; Ogawa, R.; Kakugo, A.; Osada, Y.; Gong, J.P. Dynamic Cell Behavior on Synthetic Hydrogels with Different Charge Densities. *Soft Matter* **2009**, *5*, 804–1811. [[CrossRef](#)]
155. Chen, Y.M.; Yang, J.J.; Osada, Y.; Gong, J.P. Synthetic Hydrogels as Scaffolds for Manipulating Endothelium Cell Behaviors. *Chin. J. Polym. Sci.* **2011**, *29*, 23–41. [[CrossRef](#)]
156. Wolf, K.J.; Kumar, S. Hyaluronic Acid: Incorporating the Bio into the Material. *ACS Biomater. Sci. Eng.* **2019**, *5*, 3753–3765. [[CrossRef](#)] [[PubMed](#)]
157. Wang, W.; Chen, S.; Zhang, L.; Wu, X.; Wang, J.; Chen, J.F.; Le, Y. Poly(lactic acid)/Chitosan Hybrid Nanoparticles for Controlled Release of Anticancer Drug. *Mater. Sci. Eng. C* **2015**, *46*, 514–520. [[CrossRef](#)] [[PubMed](#)]
158. Yoon, J.Y.; Kim, J.J.; El-Fiqi, A.; Jang, J.H.; Kim, H.W. Ultrahigh Protein Adsorption Capacity and Sustained Release of Nanocomposite Scaffolds: Implication for Growth Factor Delivery Systems. *RSC Adv.* **2017**, *7*, 16453–16459. [[CrossRef](#)]
159. Sánchez Naranjo, J.C. Fisiología Del Condrocito Articular. *Rev. Colomb. Reumatol.* **2008**, *15*, 21–33.
160. Tripathi, A.; Melo, J.S. Preparation of a Sponge-like Biocomposite Agarose-Chitosan Scaffold with Primary Hepatocytes for Establishing an In Vitro 3D Liver Tissue Model. *RSC Adv.* **2015**, *5*, 30701–30710. [[CrossRef](#)]
161. Nilsson, K. *Microcarrier Cell Culture: Principles and Methods*; 18-1140-62 Edition AA; GE Healthcare Life Sciences: Amersham, UK, 2013.
162. Khan, M.A.; Cantù, E.; Tonello, S.; Serpelloni, M.; Lopomo, N.F.; Sardini, E. A Review on Biomaterials for 3D Conductive Scaffolds for Stimulating and Monitoring Cellular Activities. *Appl. Sci.* **2019**, *9*, 961. [[CrossRef](#)]
163. Jin, G.; Li, K. The Electrically Conductive Scaffold as the Skeleton of Stem Cell Niche in Regenerative Medicine. *Mater. Sci. Eng. C* **2015**, *45*, 71–681. [[CrossRef](#)]

164. Martínez-Moreno, D.; Jiménez, G.; Chocarro-Wrona, C.; Carrillo, E.; Montañez, E.; Galocha-León, C.; Clares-Naveros, B.; Gálvez-Martín, P.; Rus, G.; de Vicente, J.; et al. Pore Geometry Influences Growth and Cell Adhesion of Infrapatellar Mesenchymal Stem Cells in Biofabricated 3D Thermoplastic Scaffolds Useful for Cartilage Tissue Engineering. *Mater. Sci. Eng. C* **2021**, *122*, 111933. [[CrossRef](#)]
165. Petitjean, N.; Canadas, P.; Royer, P.; Noël, D.; Le Floc'h, S. Cartilage Biomechanics: From the Basic Facts to the Challenges of Tissue Engineering. *Biomed. Mater. Res. Part A* **2023**, *111*, 1067–1089. [[CrossRef](#)]
166. Mishbak, H.H.; Cooper, G.; Bartolo, P.J. Development and Characterization of a Photocurable Alginate Bioink for Three-Dimensional Bioprinting. *Int. J. Bioprinting* **2019**, *5*, 189. [[CrossRef](#)] [[PubMed](#)]
167. Gao, Q.; Kim, B.S.; Gao, G. Advanced Strategies for 3D Bioprinting of Tissue and Organs Analogs Using Alginate Hydrogel Bioinks. *Mar. Drugs* **2021**, *19*, 708. [[CrossRef](#)] [[PubMed](#)]
168. Bonani, W.; Cagol, N.; Maniglio, D. Alginate Hydrogels: A Tool for 3D Cell Encapsulation, Tissue Engineering, and Biofabrication. *Adv. Exp. Med. Biol.* **2020**, *1250*, 49–61. [[PubMed](#)]
169. Pantani, R.; Sorrentino, A. Influence of Crystallinity on the Biodegradation Rate of Injection-Moulded Poly(lactic acid) Samples in Controlled Composting Conditions. *Polym. Degrad. Stab.* **2013**, *98*, 1089–1096. [[CrossRef](#)]

Disclaimer/Publisher's Note: The statements, opinions and data contained in all publications are solely those of the individual author(s) and contributor(s) and not of MDPI and/or the editor(s). MDPI and/or the editor(s) disclaim responsibility for any injury to people or property resulting from any ideas, methods, instructions or products referred to in the content.